COHESIVE ZONE MODELING FOR PREDICTING INTERFACIAL DELAMINATION IN MICROELECTRONIC PACKAGING

A Thesis
Presented to
The Academic Faculty

by

William E. R. Krieger

In partial Fulfillment
of the Requirements for the Degree
Master of Science in the
Woodruff School of Mechanical Engineering

Georgia Institute of Technology
May 2014

COHESIVE ZONE MODELING FOR PREDICTING INTERFACIAL DELAMINATION IN MICROELECTRONIC PACKAGING

Approved by:

Dr. Suresh K. Sitaraman, Advisor
School of Mechanical Engineering
Georgia Institute of Technology

Dr. Kyriaki Kalaitzidou
School of Mechanical Engineering
Georgia Institute of Technology

Dr. Shuman Xia
School of Mechanical Engineering
Georgia Institute of Technology

Dr. Torsten Hauck
Manager, Thermal/Mechanical Simulation
Freescale Semiconductor

Date Approved: March 31, 2014

ACKNOWLEDGEMENTS

I would like to thank my adviser Dr. Suresh Sitaraman, for his invaluable guidance and support throughout my time at *Georgia Institute of Technology*. Also, thanks are due to Dr. Kyriaki Kalaitzidou, Dr. Shuman Xia, and Dr. Torsten Hauck for serving on my thesis committee and providing important feedback.

I would like to acknowledge the funding support by the *Semiconductor Research Corportation*. Frequent interactions and discussion with industry liaisons Torsten Hauck, Vijay Sarijan, and Ilko Schmadlak from *Freescale Semiconductor* were also helpful in enhancing the overall quality of this research.

A special thank you is extended to my colleague Sathyanarayanan Raghavan, who has repeatedly made time to lend a helping hand.

I would like to thank my friends who have made my time at *Georgia Institute of Technology* enjoyable and memorable. Lastly, I would like to thank my parents for their endless love and support over the years.

TABLE OF CONTENTS

LIST OF TABLES

LIST OF FIGURES

NOMENCLATURE

Acronyms:

2D: two-dimensional

CCT: crack closure technique

CTE: coefficient of thermal expansion

CZ: cohesive zone

DCB: double cantilever beam

EMC: epoxy mold compound

ENF: end notched flexure

FEM: finite element modeling

FPB: four-point bend

LEFM: linear elastic fracture mechanics

SIF: stress intensity factor

SERR: strain energy release rate

SOIC: small-outline integrated circuit

VCCT: virtual crack closure technique

Symbols:

δ_C: cohesive zone critical displacement

ε: bimaterial constant

v: Poisson's ratio

σ_{max}: cohesive zone maximum traction

ψ: mode-mixity

Π: potenti*a*l energy of an elastic body

a: crack length

A: crack area

D: cohesive zone damage parameter

E: elastic modulus

G: strain energy release rate

G_I: mode I strain energy release rate

G_{II}: mode II strain energy release rate

G_C: critical strain energy release rate

J: J-Integral

K: stress intensity factor

K_I: mode I stress intensity factor

K_{II}: mode II stress intensity factor

K_{IC}: critical stress intensity factor or fracture toughness

P_{crit}: critical load value for delamination

SUMMARY

Multi-layered electronic packages continue to increase in complexity with demands for greater functionality. Interfacial delamination remains a prominent failure mechanism due to mismatch of coefficient of thermal expansion. Numerous studies have investigated interfacial cracking in on-chip and off-chip interfaces in microelectronic packages. These studies commonly use classical interfacial fracture mechanics analyses which require some knowledge of starter crack locations and crack propagation paths. Cohesive zone theory has been identified as an alternative method for modeling crack propagation and delamination without the need for a pre-existing crack. In a cohesive zone approach, traction forces between surfaces are related to the crack tip opening displacement and are governed by a traction-separation law. Unlike traditional fracture mechanics approaches, cohesive zone analyses can predict starter crack locations and directions or simulate complex geometries with more than one type of interface.

In a cohesive zone model, cohesive zone elements are placed along material interfaces. Deformation and separation of these elements under mixed-mode loading conditions are guided by traction-separation laws. Parameters that define these laws must be experimentally determined to be able to predict delamination propagation in a microelectronic package. The objective of this work is to study delamination propagation in a copper/mold compound interface through cohesive zone modeling. Mold compound and copper samples are fabricated, and such samples are used in experiments such as a four-point bend test and double cantilever beam test to obtain the cohesive zone model parameters for a range of mode mixity. The developed cohesive zone elements are then

placed in a small-outline integrated circuit (SOIC) package model at the interface between a thermoset epoxy mold compound and a copper leadframe. The package is simulated to go through thermal profiles associated with the fabrication of the package, and the potential locations for delamination are determined by examining the damage parameter of the cohesive zone elements. Design guidelines are developed to reduce mold compound/copper leadframe interfacial delamination.

CHAPTER 1

INTRODUCTION

Miniaturization and rising performance demands have led to the introduction of multilayered structures in modern microelectronic packages. During fabrication and assembly processes, these multilayered systems are subjected to several thermal excursions. During such thermal excursions, thermo-mechanical stresses develop due to coefficient of thermal expansion mismatch among different material layers in the package, and these stresses can be high enough to result in interfacial delamination.

Over the years, fracture mechanics has become the preferred method for studying interfacial delamination because it takes crack geometry into account and avoids singularity issues involved with stressed-based approaches. But fracture mechanics is limited since it requires knowledge of a pre-existing crack, and such knowledge is rarely known *a priori*.

Cohesive zone modeling is an emerging technique that can be used to study interfacial delamination. Both crack initiation and propagation may be simulated with cohesive zone modeling since no pre-existing crack is required, and multiple cracks may be simulated in one model. For these reasons, cohesive zone modeling of interfacial delamination is seen as a valuable alternative to fracture mechanics approaches.

CHAPTER 2

BACKGROUND AND MOTIVATION

Microelectronic packaging is a multi-disciplinary field that requires careful consideration of many electrical, thermal, and mechanical tradeoffs. These tradeoffs are driven by performance, cost, and reliability requirements [1]. Mechanical reliability is essentially durability: a reliable microelectronic package should perform its required function throughout its design lifetime. Reliability should be considered at all design stages to prevent package failure [2].

Interfacial delamination is one method of microelectronic package failure that is prevalent in packages with dissimilar materials. Mismatch in coefficients of thermal expansion (CTE) generates stresses along the interface between the layers during thermal excursions either due to operating environmental conditions and/or due to power cycling of devices. Therefore, multi-material interfaces are common points of delamination failure since directly bonded interfaces and adhesively bonded interfaces are generally weaker than cohesive materials. This has prompted numerous experimental [3-6] and analytical studies [7-12] of interfacial strength.

Many experimental methods are available for studying interfacial strength. Tests such as tab pull test, button shear test, single leg bending, etc. have been used to investigate interfacial fracture properties [7, 8, 13-16]. Such tests effectively compare adhesion in a qualitative sense, but quantitative results are more difficult to obtain.

For simple stacked geometries, some closed-form stress solutions are available, but these solutions are lacking in scope. For more complex geometries, solutions are

very complex, or they are unavailable. Closed-form solutions require a number of assumptions and do not normally account for temperature-, time-, and direction-dependent material properties. Often, they are limited to elastic regimes. Also, interfaces and sharp corners can produce singularity issues. For these reasons, a fracture mechanics approach is preferred over a stress-based analysis.

Fracture mechanics describes stresses in a body near a pre-existing crack tip. Knowledge of the starter crack size and location must be assumed for a fracture mechanics analysis. A parameter such as stress intensity factor (SIF) or strain energy release rate (SERR) is used to study crack propagation. Such parameters consider many factors, including loading applied, crack size and location, and material properties. If the parameter exceeds the critical SIF or the critical SERR, the crack is expected to propagate. Analytical calculations of fracture mechanics parameters are frequently difficult, especially when the geometry is complex or when the material behavior is temperature- and direction-dependent or inelastic. In such situations, finite element modeling (FEM) is commonly used as a tool for fracture mechanics analysis.

Critical SERR measurements have been used to perform classical fracture mechanics analyses of interfacial delamination to improve mechanical reliability in microelectronic packaging [17-20]. FEM is used to create a model of a package such as small outline integrated circuit (SOIC) package or flip-chip package, and a starter crack of known geometry and size is modeled at a probable failure region. Appropriate loading is applied. SERR is obtained from well-known methods like virtual crack closure technique (VCCT), virtual crack extension technique, J-integral, etc. [e.g. 17, 18, 21, 22, 23]. The crack is expected to grow if the SERR exceeds the critical SERR.

Fracture mechanics is adequate for analyzing geometries with well-known starter crack locations. Crack propagation can be simulated with FEM using nodal release techniques, but several iterations are required to re-check failure criteria as the crack grows. Also, fracture mechanics does not describe crack initiation, and analyses must be repeated several times to simulate different starter crack geometries. In any case, fracture mechanics involves several unknowns since starter crack size and geometry are rarely known *a priori*.

Cohesive zone (CZ) modeling is an emerging technology capable of simulating crack initiation and crack propagation with multiple crack locations in one model. With these advantages, CZ modeling has been identified as a highly useful technique for studying interfacial delamination in microelectronic packaging to improve mechanical reliability. Interfacial fracture experiments and CZ models have been used to simulate several types of interface, including integrated thin-film structures, adhesively bonded polymers, glass/elastomer, and on-chip interfaces [24-27]. In this work, cohesive zone modeling is used to study interfacial delamination in a copper leadframe/epoxy molding compound (EMC) interface with the goal of improving mechanical reliability.

A fully defined cohesive zone model of a copper/EMC interface may be inserted into models of microelectronic packages with such an interface, like small-outline integrated circuit (SOIC), flip-chip, or stacked IC packages. With CZ elements, the package model is a predictive model that can be used to simulate various conditions and determine if interfacial cracking will occur. This work will fully define a CZ model for a copper/EMC interface and insert CZ elements into an SOIC model at the interface between copper leadframe and epoxy molding compound.

CHAPTER 3

OBJECTIVES AND SCOPE OF THE RESEARCH

Computer simulation tools have become a fundamental tool for studying and preventing interfacial delamination in microelectronic packaging. Fracture mechanics approaches have been successful, but such techniques have several limitations. Fracture mechanics cannot predict crack initiation or describe geometries involving multiple cracks. Cohesive zone modeling has been identified as a solution to these limitations. Cohesive zone models may be used to study interfacial delamination, but well-defined procedures for using cohesive zone models have not yet been developed. The objectives of this thesis are to study mold compound/copper interfacial delamination through the development of cohesive zone models and to employ such models to develop design guidelines for minimizing interfacial delamination in a microelectronic package. Based on these objectives, the methods of this work are as outlined below:

1. Characterize the critical SERR of a copper/EMC interface by performing interfacial fracture experiments. Measure critical SERR at different mode-mixity and record load-displacement data.
2. Create 2D models of interfacial fracture experiments and determine mode-mixity through FEM to characterize critical SERR versus mode-mixity.
3. Create 2D cohesive zone models of interfacial fracture experiments. Apply critical SERR values from experiments and determine all six cohesive zone

parameters for mixed-mode interfacial delamination of a copper/EMC interface by mimicking experimental load-displacement data.

4. Create a 2D model of a typical SOIC package. Identify appropriate material models and apply thermal excursions involved in package fabrication. Use element birth and death to develop a process model of package assembly.
5. Create a starter crack in the SOIC model and use fracture mechanics techniques to evaluate SERR and compare to critical SERR obtained from experiments.
6. Create a predictive model by applying cohesive zone elements at interfaces between thermoset EMC and copper leadframe. Examine interfacial delamination to determine if the interface will fail.
7. Perform various simulations using the predictive model to evaluate the effects of various model geometries on interfacial delamination. Develop geometric design and process guidelines to reduce interfacial delamination in SOIC packages.

CHAPTER 4

LITERATURE REVIEW

Microelectronic packaging increases in complexity as demands for functionality increase, but interfacial delamination has been studied as a critical failure mode for over twenty years. The majority of electronic packages undergo numerous thermal excursions over a lifetime. As a result, thermo-mechanical stresses caused by CTE mismatch cannot be avoided. Several tools are available to investigate failure criteria and determine if thermo-mechanical stresses will exceed these criteria. Fracture mechanics has been used repeatedly to evaluate interfacial strength and investigate delamination propagation from various starter cracks. In reality, location and size of starter cracks are not known *a priori*. To overcome these limitations, cohesive zone modeling has been identified as a method for analyzing interfacial delamination.

4.1 Linear Elastic Fracture Mechanics

Fracture mechanics has been the dominant tool for studying interfacial delamination for many years and has been used time and time again to study die/die attach interfaces, copper leadframe/resin interfaces, copper leadframe/molding compound interfaces, and others [4]. In a fracture mechanics approach, experiments are used to quantify a failure criterion for the interface. Then package geometry is modeled, and simulated loading criteria are compared to the failure criteria. If the loading criteria exceed the failure criteria, delamination is expected to propagate.

Linear elastic fracture mechanics (LEFM) defines two parameters which are commonly used to evaluate failure criteria around a pre-existing crack or defect. Stress intensity factor and strain energy release rate have both been used effectively to analyze cracking and delamination, though recent studies have largely utilized strain energy release rate methods. In either case, fracture mechanics assumes an initial crack or defect exists in the material.

4.1.1 Stress Intensity Factor

In homogenous bodies, several studies of stress fields around a crack tip yielded a number of closed form equations describing stresses in the body, with Irwin and Orowan among the earliest [28, 29]. By defining a polar coordinate system from the crack tip, later studies found that stress fields can be generalized to vary with a single parameter, defined as the stress intensity factor (SIF), represented by K. K is given a subscript to determine the mode of loading. Fig. 4.1 shows the modes of loading that may be applied to a crack in a 2D case. Loading that induces both normal and shear stresses near the crack tip is said to be mixed-mode.

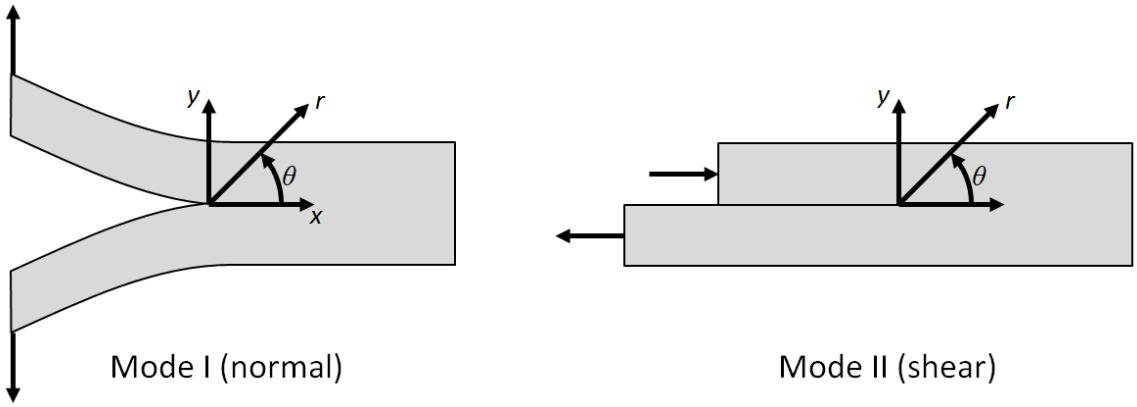

Figure 4.1: Loading modes for a 2D cracked geometry.

The stress field ahead of a crack tip for mode I loading can be described by the following equations [30].

$$\sigma_{xx} = \frac{K_I}{\sqrt{2\pi r}} \cos\left(\frac{\theta}{2}\right)\left[1 - \sin\left(\frac{\theta}{2}\right)\sin\left(\frac{3\theta}{2}\right)\right] \tag{4.1}$$

$$\sigma_{yy} = \frac{K_I}{\sqrt{2\pi r}} \cos\left(\frac{\theta}{2}\right)\left[1 + \sin\left(\frac{\theta}{2}\right)\sin\left(\frac{3\theta}{2}\right)\right]$$

$$\tau_{xy} = \frac{K_I}{\sqrt{2\pi r}} \cos\left(\frac{\theta}{2}\right)\sin\left(\frac{\theta}{2}\right)\cos\left(\frac{3\theta}{2}\right)$$

The equations give normal stresses in the *x* and *y* directions (σ_{xx}, σ_{xx}) and *x*-*y* shear stress (τ_{xy}). r and θ are polar coordinates shown in Fig. 4.1. K_I is the mode I SIF. The stress field ahead of a crack tip for mode II loading is described by the following equations [30].

$$\sigma_{xx} = -\frac{K_{II}}{\sqrt{2\pi r}} \sin\left(\frac{\theta}{2}\right)\left[2 + \cos\left(\frac{\theta}{2}\right)\cos\left(\frac{3\theta}{2}\right)\right] \tag{4.2}$$

$$\sigma_{yy} = \frac{K_{II}}{\sqrt{2\pi r}} \sin\left(\frac{\theta}{2}\right)\cos\left(\frac{\theta}{2}\right)\cos\left(\frac{3\theta}{2}\right)$$

$$\tau_{xy} = \frac{K_{II}}{\sqrt{2\pi r}} \cos\left(\frac{\theta}{2}\right)\left[1 - \sin\left(\frac{\theta}{2}\right)\sin\left(\frac{3\theta}{2}\right)\right]$$

Similarly, K_{II} is the mode II stress intensity factor. Thus, the stress field magnitudes for 2D problems are completely defined by K_I and K_{II}. Stress field solutions

may be superimposed to obtain stresses near the crack tip for mixed mode loading conditions.

K can be calculated analytically as a function of far-field stress and crack length for several known loading configurations for cracked structures. Homogenous materials tend to crack under pure mode I conditions, so the critical value which causes fracture is known as critical stress intensity factor K_{IC}. Critical SIF is a material property that can be measured through fracture experiments. Then if *K* exceeds K_{IC} in any cracked body of the same material, the crack will propagate.

4.1.2 Strain Energy Release Rate

In an energy-based fracture mechanics approach, strain energy release rate (SERR) is used to analyze crack growth. To extend a crack, energy input is required to create two new surfaces of unit area within the material. The rate of change of this energy with respect to crack area is defined as SERR *G*. Another interpretation of *G* is the energy available from applied loading for the crack to propagate. Irwin defined energy release rate as a modified form of the Griffith energy balance, where Π is the potential energy stored within an elastic body and *A* is the crack area [30]:

$$G = -\frac{d\Pi}{dA} \tag{4.3}$$

For linear elastic fracture mechanics, *G* varies directly with K_I^2 according to the following equation [30]:

$$G = \frac{K_I^2}{E} \quad \text{plane stress} \tag{4.4}$$

$$G = \frac{K_I^2(1-\nu^2)}{E} \quad \text{plane strain}$$

Similar to the stress intensity factor method for analyzing crack growth, crack extension occurs when G reaches a critical value, known as critical strain energy release rate G_C. Like K_{IC}, G_C is a material property for cohesive materials. If G exceeds G_C in any geometry, the crack will propagate.

4.1.3 Virtual Crack Closure Technique

In many cases, closed form equations of SERR are available for known geometries. For simple geometries, such as fracture toughness test geometries, formulas may be derived from classical beam theory, energy balances, or from SIF analyses. But in cases where equations are difficult to derive analytically, numerical solutions are available. Several techniques for SERR measurement are implemented in FEM software, including virtual crack extension, virtual crack closure, and J-integral techniques, all of which have been shown to produce comparable results [31]. For this work, virtual crack closure technique (VCCT) is utilized to calculate SERR for interfacial fracture tests.

The crack closure technique was developed by Rybicki and Kanninen [32]. To apply VCCT, a crack tip is incorporated into an FEM model. VCCT theory does not require crack tip singularity elements to capture crack tip behavior. In a 2D case, a crack tip is constructed in the model by leaving nodes uncoupled along a crack length a. Crack tip geometry is shown in Fig. 4.2. Elements are eight node quadratic elements.

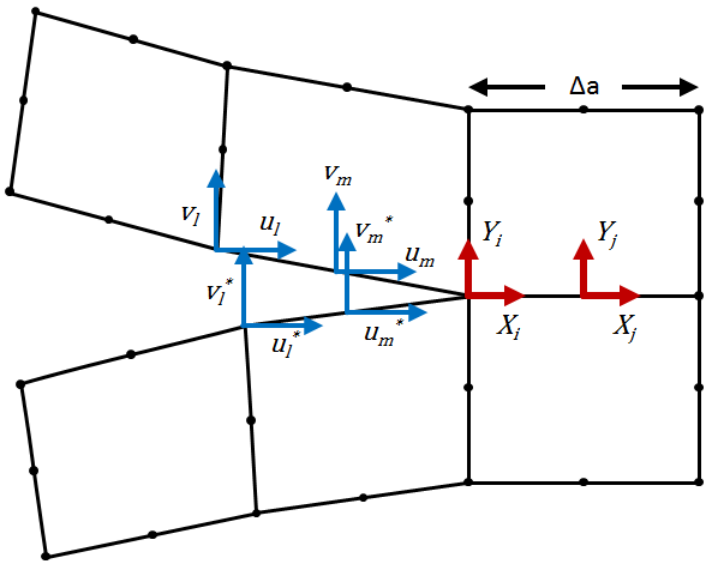

Figure 4.2: Crack tip geometry for VCCT calculations.

VCCT assumes that as the crack extends from length a to $a + \Delta a$, the state of the crack tip remains unchanged [32, 33]. In other words, crack tip opening displacements and forces at the crack tip are presumed to be identical for small Δa. Therefore, the energy released by extending the crack by Δa is equivalent to the energy required to close the crack along a length Δa. The following equations are used to calculate G using eight node elements [33].

$$G_I = -\frac{1}{2\,\Delta\,a}\left[Y_i(v_l - v_l^*) + Y_j(v_m - v_m^*)\right] \tag{4.5}$$

$$G_{II} = -\frac{1}{2\,\Delta\,a}\left[X_i(u_l - u_l^*) + X_j(u_m - u_m^*)\right]$$

v and u are vertical and horizontal displacements, respectively, and Y and X are vertical and horizontal nodal forces at the crack tip. To obtain Y and X, elemental forces

are summed from the upper surface only. For the 2D case, total SERR is calculated as $G = G_I + G_{II}$.

4.1.4 J-Integral Technique

J-Integral is another technique implemented in FEM software that has been used to calculate SERR [9, 31]. The J-Integral was proposed by Rice as the energy release rate in a cracked nonlinear elastic body [10]. For a 2D case, J can be reduced to a path-independent line integral around the crack tip as follows [30].

$$J = \int_{\Gamma} \left(w dy - T_i \frac{\partial u_i}{\partial x} ds \right) \tag{4.6}$$

J is the path-independent nonlinear energy release rate along a contour Γ. w is the strain energy density, the traction vector has components T_i, and u_i are displacement vector components. Since J-Integral considers nonlinear effects, it can be used to analyze cracking with elastic-plastic materials. For the elastic case, J is equivalent to G.

4.1.5 Interfacial Fracture Mechanics

All of the methods discussed up to now have described cohesive fracture behavior of homogeneous materials. Applying fracture mechanics techniques to an interfacial crack between dissimilar materials introduces additional challenges. A bimaterial interfacial crack is shown in Fig. 4.3.

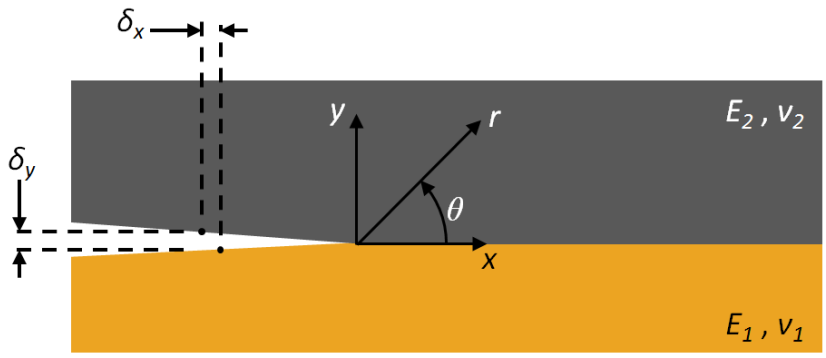

Figure 4.3: A bimaterial crack between two dissimilar materials.

The bimaterial fracture problem was first solved analytically by Williams, who determined the stresses surrounding a singularity at a sharp crack tip [34]. An interfacial crack is described by the bimaterial constant ε, calculated by (4.7) [35].

$$\varepsilon = \frac{1}{2\pi}\ln\left(\frac{1-\beta}{1+\beta}\right) \tag{4.7}$$

$$\beta = \frac{\mu_1(\zeta_2-1)-\mu_2(\zeta_1-1)}{\mu_1(\zeta_2+1)+\mu_2(\zeta_1+1)}$$

ε is the bimaterial constant and β is one of the Dundur's parameters. A greater magnitude of ε indicates less similar materials. In a homogenous material, $\varepsilon = \beta = 0$. Subscripts in equation (4.7) refer to materials in Fig. 4.3. μ_i are shear moduli where $\mu_i = E_i/[2(1 + \nu_i)]$, and for plane strain $\zeta_i = (3 - 4\nu_i)$. Due to the dissimilarity of materials, an interface crack experiences mixed mode conditions even when pure mode I loading is applied [35]. The SIF stress field solution for bimaterial fracture is given by (4.8) [21].

For linear elastic materials, VCCT and J-integral calculations are valid for bimaterial interfacial fracture.

$$\sigma_y + i\sigma_{xy} = \frac{1}{\sqrt{2\pi r}}(K_I^* + iK_{II}^*)r^{i\varepsilon} \tag{4.8}$$

$K = K_I^* + iK_{II}^*$ is a complex stress intensity factor that does not represent opening and shear modes strictly for the bimaterial problem. Thus, unlike homogenous fracture, interfacial fracture is heavily dependent on mode-mixity ψ.

4.1.6 Mode-mixity For Interfacial Fracture

Several studies have investigated analytical and numerical methods for evaluating mode-mixity at a bimaterial interface. Interfacial mode-mixity is defined as the relative proportions of shear to normal tractions ahead of the crack tip [35]. There is abundant evidence that critical SERR depends strongly on mode-mixity [7, 36].

Analytical methods for calculating mode-mixity have been proposed (e.g. Hutchinson and Suo), but they are mathematically complex [37]. Numerical methods include crack-surface displacement method, M-integral method, or modified VCCT results [9, 38]. For this work, the crack-surface displacement method proposed by Matos et al. is used to calculate mode-mixity [9].

Crack-surface displacement method uses crack opening displacements from FEM at a distance from the crack tip. Hutchinson and Suo describe crack displacement jumps by (4.9) [35].

$$\delta_y + i\delta_x = 8\frac{K_I^* + iK_{II}^*}{(1+i2\varepsilon)E^*\cosh(\pi\varepsilon)\sqrt{2\pi}}\sqrt{r}\left(\frac{r}{l}\right)^{i\varepsilon} \tag{4.9}$$

$$\frac{1}{E^*} = \frac{1}{2}\left(\frac{1}{\overline{E_1}} + \frac{1}{\overline{E_2}}\right)$$

Vertical and horizontal crack displacements δ_y and δ_x (Fig. 4.3) are calculated at a distance r from the crack tip. K_I* and K_{II}* are components of the complex bimaterial SIF, and ε is the bimaterial constant. 1/E* is calculated as the average compliance of the two materials using plane strain moduli, where the plane strain moduli are given by $\overline{E_i} = E_i/(1 - \nu_i^2)$. l is a characteristic length used to normalize the crack tip distance, typically chosen to be specimen width or thickness.

Crack surface displacements are obtained from a finite element model and mode-mixity is calculated as follows [35].

$$\psi = \arctan\left(\frac{\delta_x}{\delta_y}\right) - \arctan(-2\varepsilon) - \varepsilon\ln\left(\frac{r}{l}\right) \tag{4.10}$$

ψ is calculated at a distance r which best satisfies (4.11) [35]. In plots, the left side of (4.11) is referred to as δ^2/r, and the right side is referred to as G*.

$$\frac{\delta_y^2 + \delta_x^2}{r} = 64\frac{G}{2\pi(1+4\varepsilon^2)E^*} \tag{4.11}$$

First, G is calculated through VCCT. Since all other parameters on the right side of (4.11) are known, the right side is a constant. Then using FEM, several displacements δ_x and δ_y are obtained at varying distance r from the crack tip. Both sides of (4.11) are plotted, and r is selected where the curves intersect. At this distance r, δ_x and δ_y are used with (4.10) to calculate ψ.

For characterizing G_C across a range of ψ, Hutchinson and Suo present a model in (4.12), where $G_{I,C}$ is the critical SERR at zero mode-mixity, and λ is a non-dimensional parameter for fitting the model [37].

$$G_C = G_{I,C}[1 + \tan^2(\psi(1 - \lambda))] \tag{4.12}$$

4.2 Cohesive Zone Model

Cohesive zone (CZ) modeling is an emerging technology capable of simulating crack initiation in addition to crack propagation. Therefore, a major advantage of cohesive zone theory over fracture mechanics theory is that CZ analysis does not require knowledge of starter crack size and geometry. CZ models have been used to simulate several types of interfaces, including integrated thin-film structures, adhesively bonded polymers, glass/elastomer, and on-chip interfaces [24-27]. Here we apply a CZ technique to model delamination between copper leadframe and epoxy molding compound (EMC).

4.2.1 Cohesive Zone Cracking

In a CZ model, interfacial separation occurs within a cohesive damage zone when the damage exceeds a pre-set limit. Within the cohesive zone, there are active traction

stresses between the cohesive surfaces, and interaction is governed by a traction-separation law. Before loading is applied, a CZ zone element is said to be undamaged, while a fully damaged element has been completely separated, and does not produce any force interactions between the cohesive surfaces. Fig. 4.4 shows a cohesive zone model for interfacial separation.

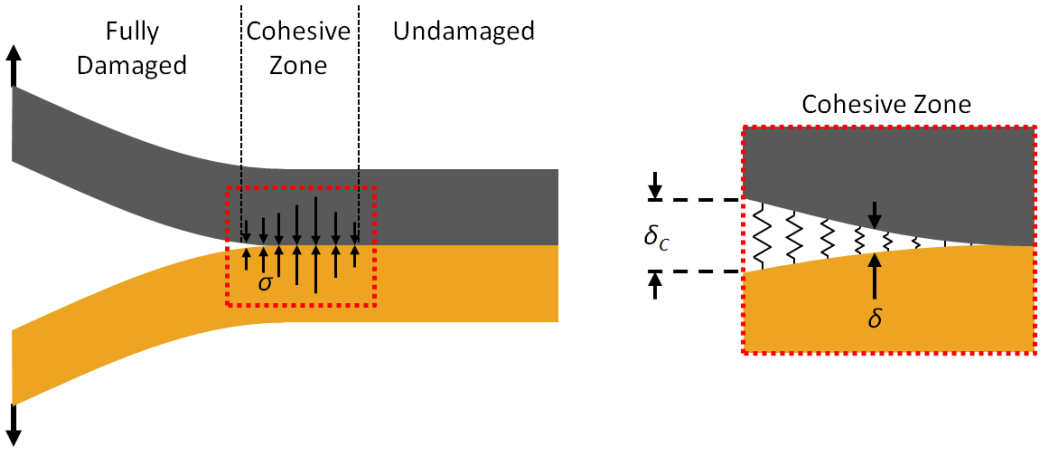

Figure 4.4: Cohesive zone model of interfacial separation.

The traction σ is exerted by the interface until the interfacial separation δ reaches a critical value δ_C. σ is a function of δ given by traction-separation law. As the element becomes damaged, the area beneath the traction-separation law is the mechanical work needed to separate the element. Thus, the area beneath the traction-separation law is equivalent to G_C. Several shapes of CZ law are available for describing material behaviors, as seen in Fig. 4.5, such as bilinear, exponential, trapezoidal, and trilinear [25, 39]. Such laws allow for cohesive zone elements to model a wide range of material

behavior, including the potential for modeling nonlinear behaviors that cannot be captured with fracture mechanics.

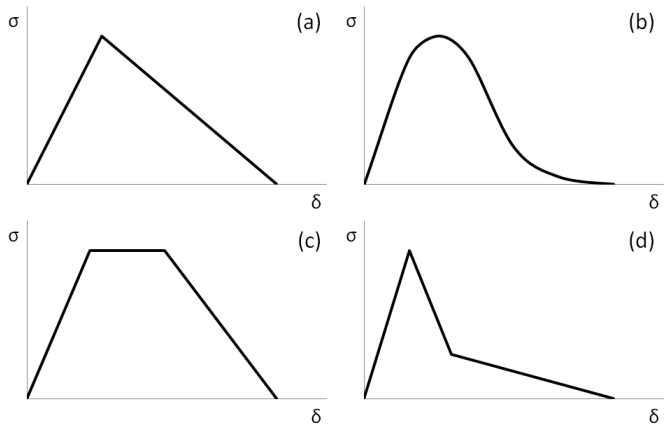

Figure 4.5: Available traction-separation laws for cohesive zone models, including (a) bilinear, (b) exponential, (c) trapezoidal, and (d) trilinear laws.

Defining a bilinear law is nontrivial, as there is currently no way to directly measure cohesive zone parameters experimentally. Of the traction-separation laws shown in Fig. 4.5, (b), (c), and (d) require four or more parameters to fully define the cohesive zone behavior. For this work, a bilinear traction-separation law (Fig. 4.5a) is used because the curve is defined by only three parameters.

4.2.2 Bilinear Traction-Separation Law

The bilinear traction-separation law (Fig. 4.5a) was proposed by Alfano and Crisfield for modeling interfacial separation [40]. Several bimaterial interfaces have been simulated using this law, though properly defining a mixed-mode law for such interfaces remains a challenge. In this work a bilinear law (Fig. 4.6) is used to model behavior of a copper/EMC interface.

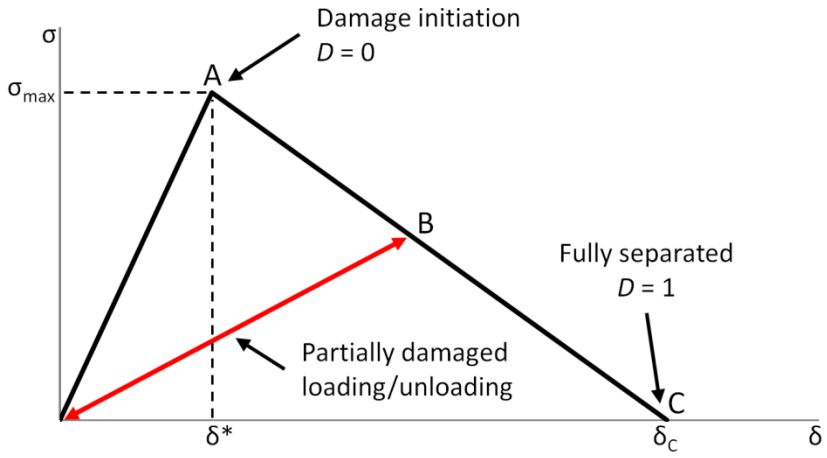

Figure 4.6: Bilinear traction-separation law for cohesive zone elements.

The bilinear law shows interfacial traction σ versus interfacial separation δ. As CZ elements undergo deformation, they exhibit elastic loading for $\delta < \delta^*$. In this region, no damage is accumulated in the interface, and unloading returns CZ elements to their initial configuration. At point A, a critical traction σ_{max} is reached and damage is initiated. Delamination is tracked by a damage parameter D calculated by (4.13). When $\delta > \delta^*$, D increases, and when $\delta \geq \delta_C$, D reaches a maximum value of 1.

$$D = \begin{cases} 0 & \text{if } \delta \leq \delta^* \\ \left(\frac{\delta - \delta^*}{\delta}\right)\left(\frac{\delta_c}{\delta_c - \delta^*}\right) & \text{if } \delta^* < \delta < \delta_c \\ 1 & \text{if } \delta \geq \delta_c \end{cases} \tag{4.13}$$

Regardless of the current magnitude of δ, the damage value D can never decrease. In other words, unloading will not reduce the damage that has accumulated. Therefore if a CZ element is unloaded while partially damaged, from point B for example, it follows a

path of reduced stiffness. When loading is resumed, the element will have the same reduced stiffness until it returns to point B, where further damage will initiate.

When the damage parameter D = 1, the CZ element is said to be fully damaged, and the stiffness of the cohesive zone element is zero. Thus, a fully damaged element has been completely separated and will not produce interactions between layers. Throughout separation, traction is a function of interfacial separation given by (4.14).

$$\sigma = \frac{\sigma_{max}}{\delta^*}(1 - D)\delta \tag{4.14}$$

As mentioned previously, the area under the traction-separation profile is the critical strain energy release rate, and thus, for the bilinear law, $G_C = 0.5\ \delta_C\ \sigma_{max}$.

4.2.3 Mixed-mode Implementation of the Bilinear Law

In applications, interfacial cracking always propagates in mixed-mode conditions [36]. Therefore, two bilinear laws are required to define mixed-mode cohesive zone behavior. The bilinear laws correspond to pure mode I and pure mode II delamination, and mixed-mode interpolation is applied by FEM software. Each bilinear law is defined by three parameters: maximum traction σ_{max}, critical displacement δ_C, and loading-unloading ratio $\alpha = \delta^*/\delta_C$, comprising six total parameters required for a mixed-mode cohesive zone model. This work presents a methodology for determining mixed-mode CZ parameters for a copper/EMC interface.

CHAPTER 5

EXPERIMENTAL CHARACTERIZATION OF THE INTERFACE

As a first step toward obtaining cohesive zone parameters, critical strain energy release rate is calculated for the copper/EMC interface. Since G_C is a function of mode-mixity, G_C must be characterized over a range of ψ for any particular interface. Researchers have demonstrated several techniques to characterize G_C at varying ψ. These include mixed-mode bend, end-notched flexure, double cantilever beam, four-point bend, superlayer, and magnetic actuation [16, 19, 31, 41-46]. For this work, double cantilever beam and four-point bend tests are used. Load-displacement data is recorded and will be used to determine CZ parameters.

5.1 Bimaterial Copper/EMC Specimens

Freescale Semiconductor has provided testing specimens for experimental characterization of the interface. Fig. 5.1 shows a bimaterial strip specimen. The specimens are bimaterial strip samples consisting of a layer of EMC molded directly to a copper strip. The assembly procedure is as follows. A transfer mold is clamped over a copper leadframe. Liquid encapsulant is injected into the mold and cured at 175 °C. Samples are ejected from the mold and cooled to room temperature. Materials used are CDA194 copper alloy and *Sumitomo Sumikon*® EME-G630AY molding compound. Material properties for interfacial characterization appear in Table 5.1.

Table 5.1: Material properties for bimaterial strip specimens.

	Copper	EMC
***E* [GPa]**	121	25.0
v	0.33	0.30

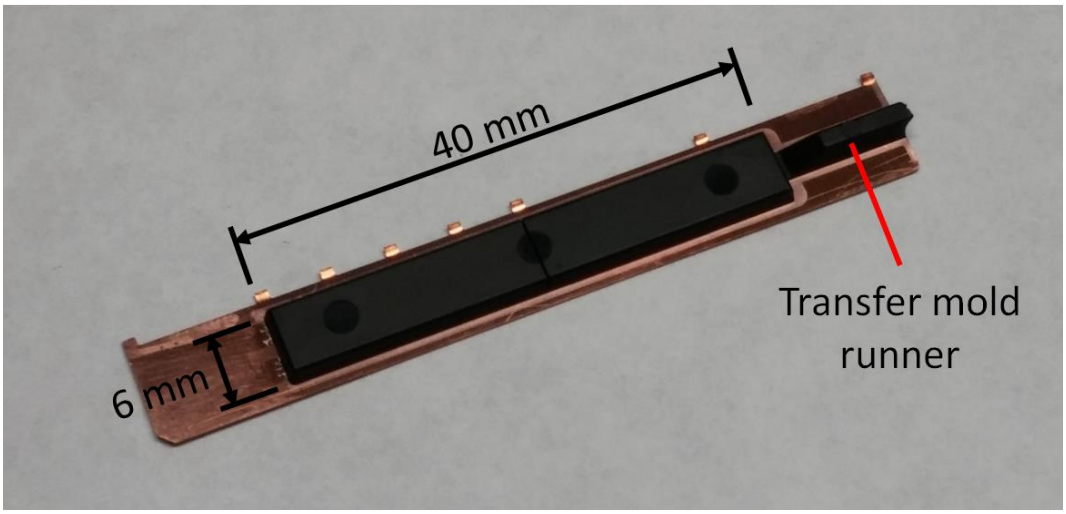

Figure 5.1: Bimaterial strip specimen for experimental characterization.

In some studies, residual stresses and cure shrinkage of the EMC material may be considered in calculations of G_C. Consideration of residual stresses and cure shrinkage is expected to increase the measured value of G_C for a copper/EMC interface [43]. Therefore, the values calculated in this work without considering residual stresses and cure shrinkage are conservative measurements of critical SERR.

5.2 Double Cantilever Beam Test

The double cantilever beam (DCB) test has also been used successfully to measure critical strain energy release rate. DCB geometry replicates loading conditions

fairly close to mode I and requires loading fixtures to be attached to the specimen. Values from load-displacement data are used to calculate G_C.

5.2.1 DCB Experimental Results

A DCB test schematic appears in Fig. 5.2. Before testing a pre-crack is created in the specimen. To create the pre-crack, the specimen is clamped a known distance from the end and the free end is bent downward to initiate the delamination. Approximate pre-crack length is controlled by the placement of the crack. After the pre-crack has been created, aluminum loading fixtures are attached to the specimen using epoxy. The specimen is placed into a *Delamination Testing System* tensile test machine and fixtures are connected via two loading pins. The loading pins and fixtures are greased before assembly to prevent moments from being applied to the specimen.

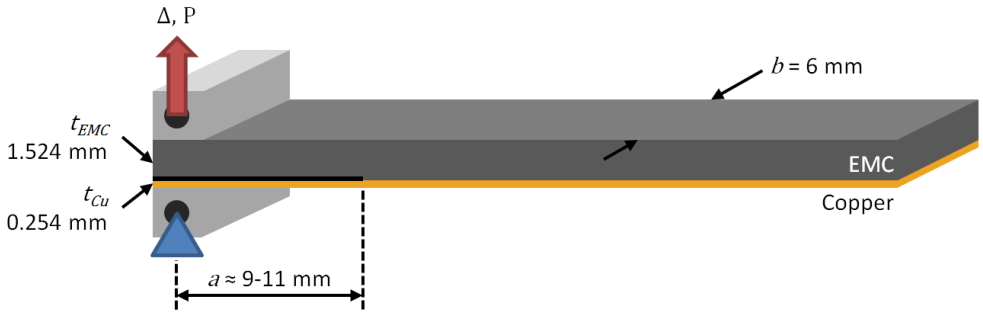

Figure 5.2: Schematic for double cantilever beam test.

Displacement-controlled loading is applied in a tensile direction at 10 μm/sec. Initially, the load is expected to increase linearly. At some critical load, load begins to decrease. Load reduction indicates delamination has propagated some distance. Although load has decreased and delamination has started to propagate, the exact crack

length needs to be determined for analytical calculations as well as for numerical models. Therefore, a loading-unloading approach is employed to determine the change in compliance and thus crack length [e.g. 27]. The unloading is expected to be linear, with increased compliance compared to the initial loading. The compliance increase confirms that the delamination has propagated. Once the linear unloading is observed, the re-loading is done. Load should again increase linearly with the same compliance as the unloading curve, until a critical load is reached, and delamination propagates further. This process is repeated four to six times. A test in progress is shown in Fig. 5.3.

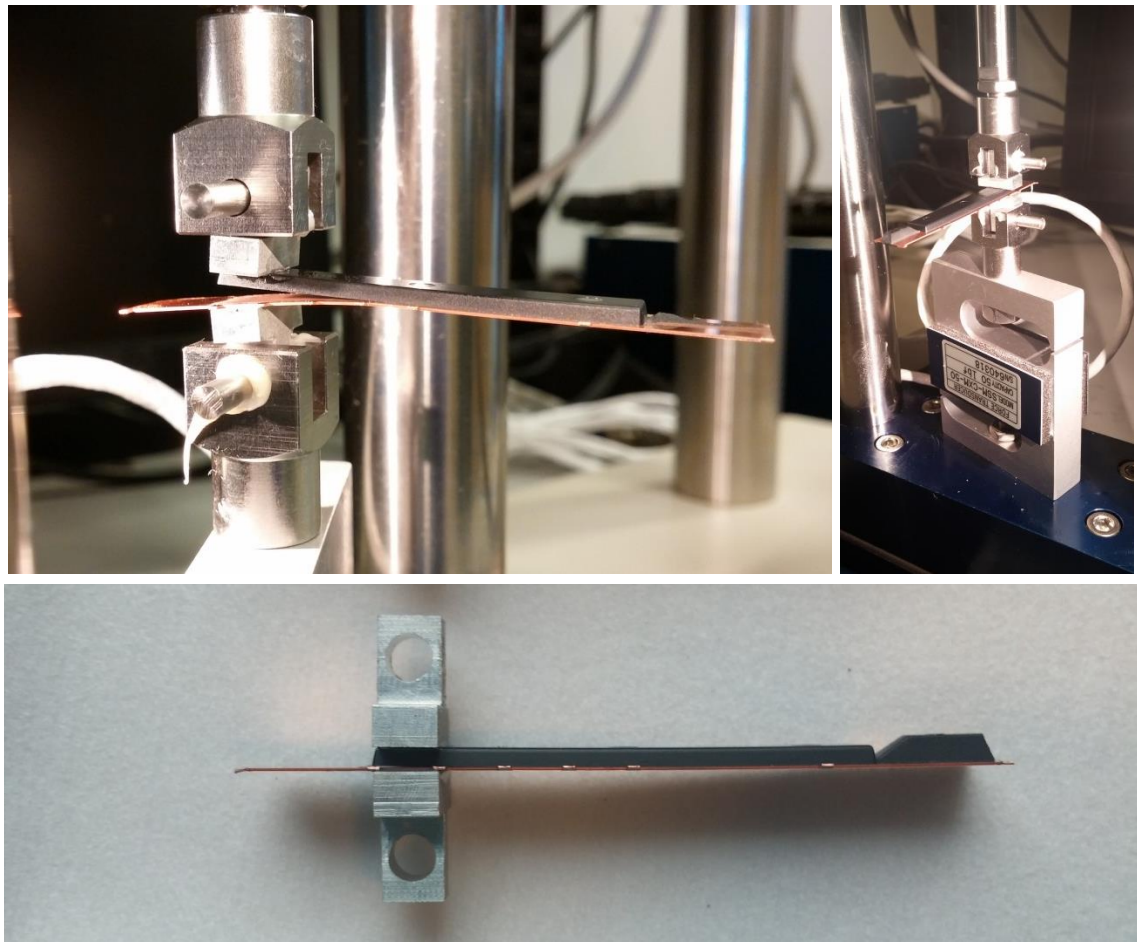

Figure 5.3: Experimental setup for double cantilever beam test.

Fig. 5.4 shows a typical load-displacement response from a specimen tested at room temperature. The specimen shows elastic bending after some initial slack in the system. The loading reaches a maximum of about 2.4 N and the load begins to decrease. At this time, the loading direction is reversed, and a linear unloading path is observed. By observation, the compliance C has increased from the initial loading, indicating delamination has propagated some distance. Loading is again reversed, and this process is repeated an additional five times. P_{crit} and C from any unloading curve can be used to calculate G_C.

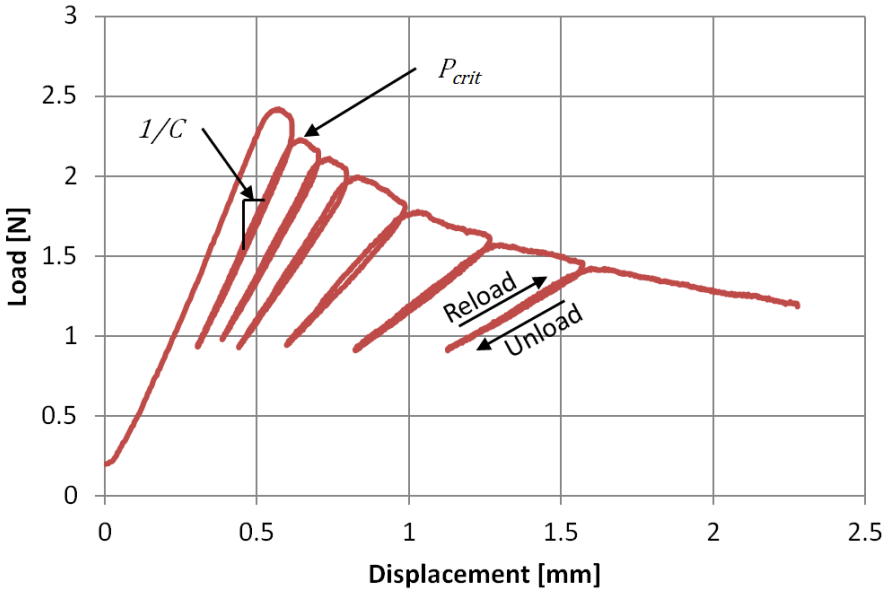

Figure 5.4: Load-displacement data from a DCB experiment.

5.2.2 DCB Analytical Calculations

For a bimaterial interface with layers of dissimilar materials, a strong analytical solution for SERR is not available. Some resources offer derivations from plate theory or

SIF analysis that result in complex equations [47, 48]. In cases where one layer is significantly thicker, the compliance method may be applied by treating the thinner layer as a single cantilever beam [5]. A modified compliance method may produce a good approximation for cracks with lengths much longer than beam thickness [48]. In this method, the layers of the DCB specimen are treated as separate cantilever beams, resulting in the following equation from Soboyejo *et al*. for mode I SERR [46].

$$G = \frac{6P^2a^2}{E_{EMC}b^2t_{EMC}^3}\left(1 + \frac{1}{\beta_E\beta_T^3}\right) \tag{5.1}$$

$$\beta_E = \frac{E_{Cu}}{E_{EMC}} \qquad \beta_T = \frac{t_{Cu}}{t_{EMC}}$$

G is the strain energy release rate for mode I loading produced by the DCB loading configuration from applied load *P*. From Fig. 5.2, *a* is the crack length and *b* is specimen width. β_E is the stiffness ratio between copper and EMC, and β_T is the thickness ratio. Material property *E* appears in Table 5.1 for both materials. Knowledge of crack length *a* is required to apply this formula. Crack length will be determined by FEM modeling.

5.2.3 DCB Numerical Modeling

For the DCB test, crack length is required to calculate G_C. First, FEM is used to obtain crack length from compliance. Then G_C and ψ can be calculated.

Crack Length

To obtain crack length, a 2D plane strain model of the DCB test is prepared. The model is shown in Fig. 5.5. Copper and EMC are assumed to be linear elastic for small

deformations, and material properties from Table 5.1 are used. At the interface, nodes are left uncoupled along a preset length *a* to create a crack. The remaining nodes at the interface are coupled to form the interface. One node is fixed at the lower surface to represent the fixed loading pin. A vertical displacement is applied to one node at the upper loading pin. Initial simulations show that interfacial stresses are primarily tensile and no material inter-penetration occurs, so contact pairings are not necessary for the DCB model.

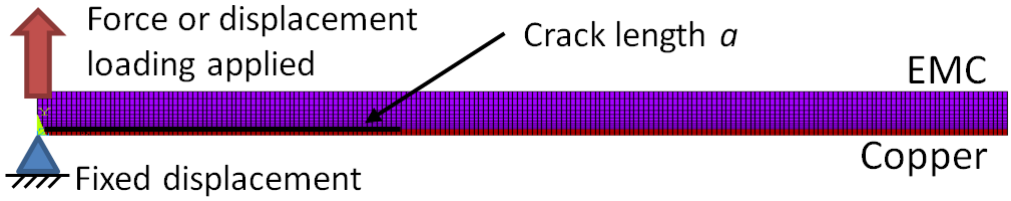

Figure 5.5: 2D model of DCB test.

The simulation is performed for several crack lengths for 3 mm < *a* < 15 mm and compliance *C* = displacement/force is recorded for each simulation. The result is a plot of compliance versus crack length, shown in Fig. 5.6. Least squares regression is used to obtain compliance as a cubic function of crack length. Crack lengths used for calculations are summarized in Table 5.2.

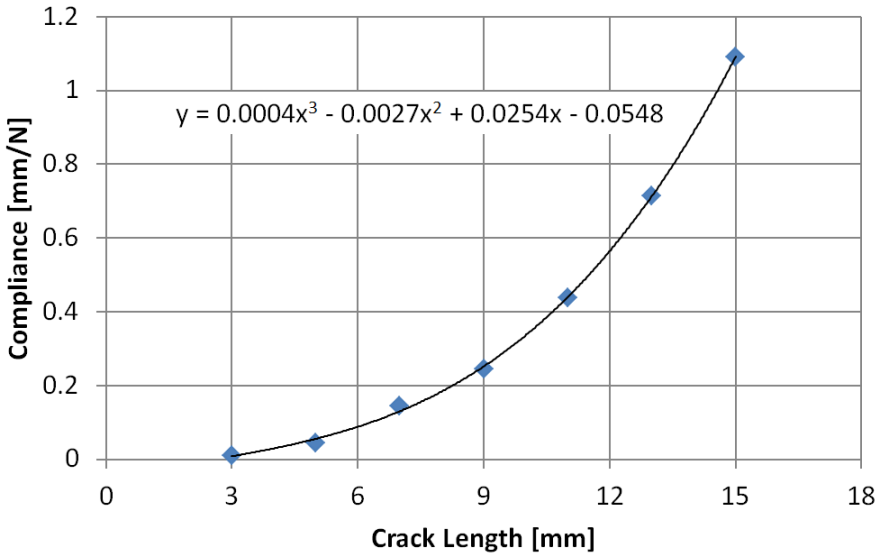

Figure 5.6: Simulated DCB compliance versus crack length.

Critical Strain Energy Release Rate

To obtain G_C, results from several unloading curves in Fig. 5.4 will be averaged. For example, in the first unloading path shown, least squares regression gives a compliance of 0.246 mm/N. This value is applied to the cubic function in Fig. 5.6, yielding a = 9.00 mm. The subsequent critical force from Fig. 5.4 is P_{crit} = 2.23 N.

The model in Fig. 5.5 is rebuilt with crack length a = 9 mm. As the P_{crit} is known for this crack length, the model is re-run, where a force equivalent to P_{crit} = 2.23 N is applied on the top pin of the DCB specimen. The critical force is divided by the specimen width since the model is 2D. With these loading conditions, the calculated G will be equivalent to G_C. The deformed model is shown in Fig. 5.7.

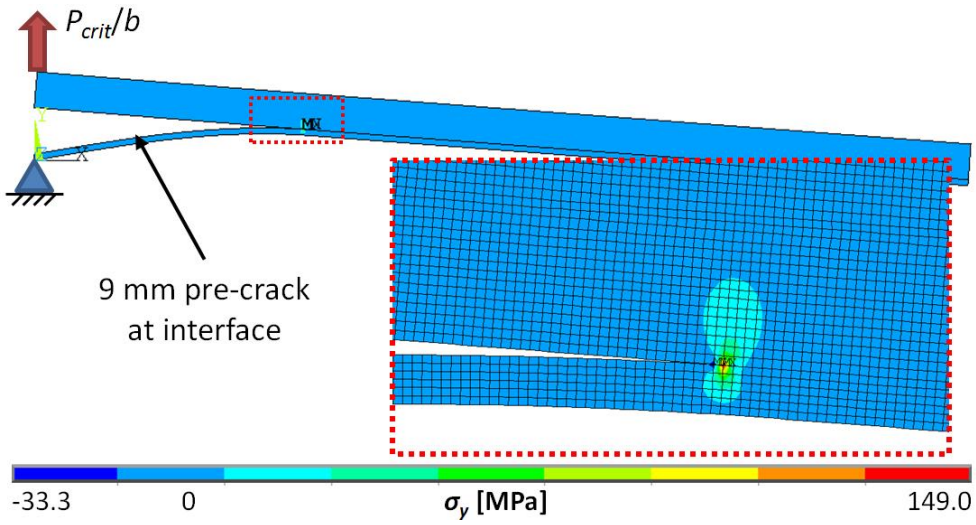

Figure 5.7: Deformed 2D model of DCB test used for calculating G_C and ψ.

The peel stress (σ_y) plot forms a familiar shape around the crack tip. The stresses vary with both angle and distance from the crack tip, as described by (4.8). Unlike a homogenous cracked body, the stress contours are not symmetric about the x-axis. To determine if yielding occurs in the copper, von mises stress is plotted, and the maximum value in the copper is 304 MPa. This value is below the material yield stress, so the linear elastic material assumption is valid.

The VCCT method is applied to the deformed model to calculate mode I and mode II energy release rates. From the three specimens, several data points are selected with various crack lengths, and Table 5.2 shows G_C from VCCT. VCCT returns an average G_C = 35.6 J/m^2.

Table 5.2: G_C calculated for the DCB test.

C [mm/N]	a [mm]	P_{crit} [N]	G_C [J/m^2]
0.260	9.18	2.2814	35.6
0.367	10.4	2.0368	36.2
0.370	10.4	2.0736	37.5
0.385	10.6	1.9358	33.9
0.467	11.3	1.8376	34.6

Using the first pairing of values for a and P_{crit} from Table 5.2, the analytical expression (5.1) returns 37.69 J/m^2. Since the analytical expression assumes that all of the P_{crit} applied contributes to mode I loading, the result is a slight overestimate of G_C, confirming the results obtained through VCCT.

Mode-Mixity

Mode-mixity is obtained through the crack displacement method. From Fig. 5.7, crack displacements are obtained at varying distances from the crack tip. Both sides of (4.11) are plotted in Fig. 5.8. The curves intersect at r = 0.016 mm, so ψ is calculated at this distance from the crack tip. For the DCB test, ψ = 5.26° using (4.10).

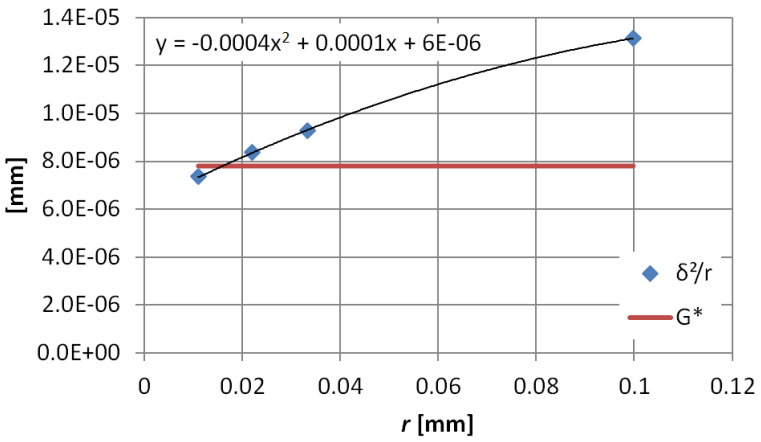

Figure 5.8: Determination of r for DCB mode-mixity calculation.

5.3 Four-Point Bend Test

The four-point bend (FPB) test is a popular experiment for critical strain energy release rate characterization since it produces stable delamination at the interface and does not depend on crack length [7, 31, 43]. The FPB loading configuration produces a constant moment between the inner loading pins. As a result, steady-state interfacial delamination occurs, evidenced by displacement increasing at a constant critical load. This constant force P_{crit} is collected from load-displacement data for use in calculating G_C.

5.3.1 FPB Experimental Results

A FPB test schematic appears in Fig 5.9. Before testing, the mold compound is notched using a *DISCO* automatic dicing saw to initiate delamination at the interface. The notch is centered in the length of the mold compound, and the depth of cut is selected so that 100 μm of EMC remains above the copper. The specimen is placed on two fixed support pins with the EMC layer downward. The notch is centered between the fixed support pins, and the loading pins are lowered into contact with the copper. All loading and support pins have diameter 3 mm.

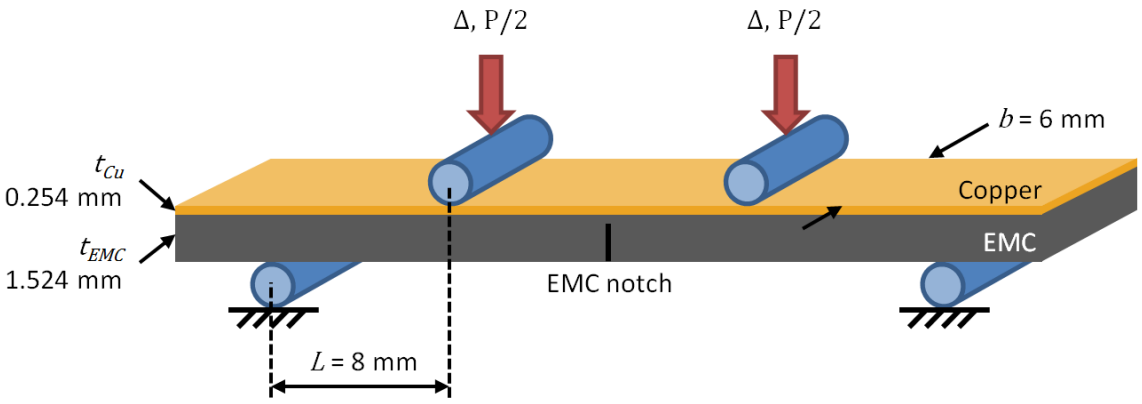

Figure 5.9: Schematic for four-point bend test.

Displacement-controlled loading is applied at a rate of 0.50 mm/min. The specimen is expected to exhibit linear load versus displacement initially. At some critical load, a crack will propagate unstably from the EMC notch to the copper/EMC interface, signaled by a load drop. Then as loading continues, delamination will propagate stably along the interface. Testing is performed on a *TestResources* tensile test machine. Load and displacement data are recorded throughout by a *TestResources* force transducer and *Epsilon Technologies* extensometer. Fig. 5.10 shows an experiment in progress.

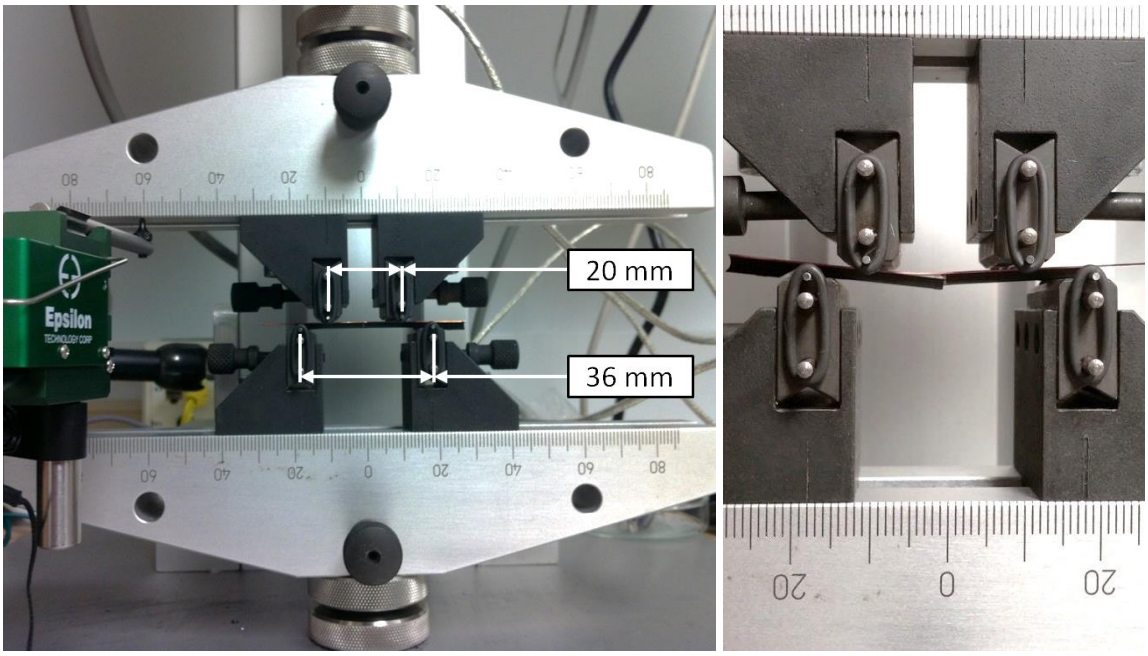

Figure 5.10: Four-point bend test in progress.

Fig. 5.11 contains a load-displacement response from one of the specimens tested at room temperature. After some initial slack in the system, the specimen shows a linear response. At a load of approximately 8.2 N, the load drops twice as a crack propagates from the EMC notch to the interface. As displacement increases, the load stabilizes, indicating interfacial delamination between EMC and copper. By comparing data from three trials, steady-state delamination can be observed at an average critical load P_{crit} = 6.25 N.

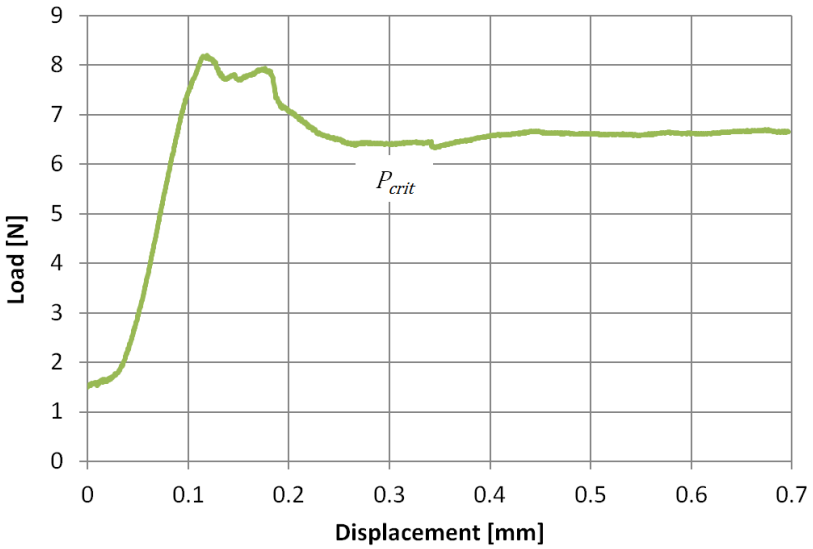

Figure 5.11: Load-displacement data from an FPB experiment.

5.3.2 FPB Analytical Calculations

For the bimaterial interface, strain energy release rate may be computed by the following equations from Charalambides *et al.* [49]. I_{Cu} is the area moment of inertia of the copper strip, while I_C is the area moment of inertia of the entire composite beam. λ is a non-dimensional parameter that gives the stiffness ratio between copper and EMC.

$$G = \frac{(1-\nu_{Cu}^2)P^2L^2}{8E_{Cu}b^2}\left(\frac{1}{I_{Cu}} - \frac{\lambda}{I_C}\right) \tag{5.2}$$

$$I_{Cu} = \frac{t_{Cu}^3}{12} \qquad \lambda = \frac{E_{Cu}(1-\nu_{EMC}^2)}{E_{EMC}(1-\nu_{Cu}^2)}$$

$$I_C = \lambda I_{Cu} + \frac{t_{EMC}^3}{12} + \frac{\lambda t_{Cu} t_{EMC}(t_{Cu}+t_{EMC})^2}{4(\lambda t_{Cu}+t_{EMC})}$$

Critical strain energy release rate G_C is obtained by calculating G during the steady-state delamination. Therefore, P_{crit} observed in experiments can be substituted into (5.2) to determine G_C. For an average P_{crit} of 6.25 N, the equation yields $G_C = 44.6$ J/m^2.

5.3.3 FPB Numerical Modeling

To calculate the mode-mixity associated with the FPB test, the VCCT method was applied using FEM. A 2D plane-strain model of the FPB test is prepared using *ANSYS*. Fig. 5.12 shows the model used for VCCT calculations.

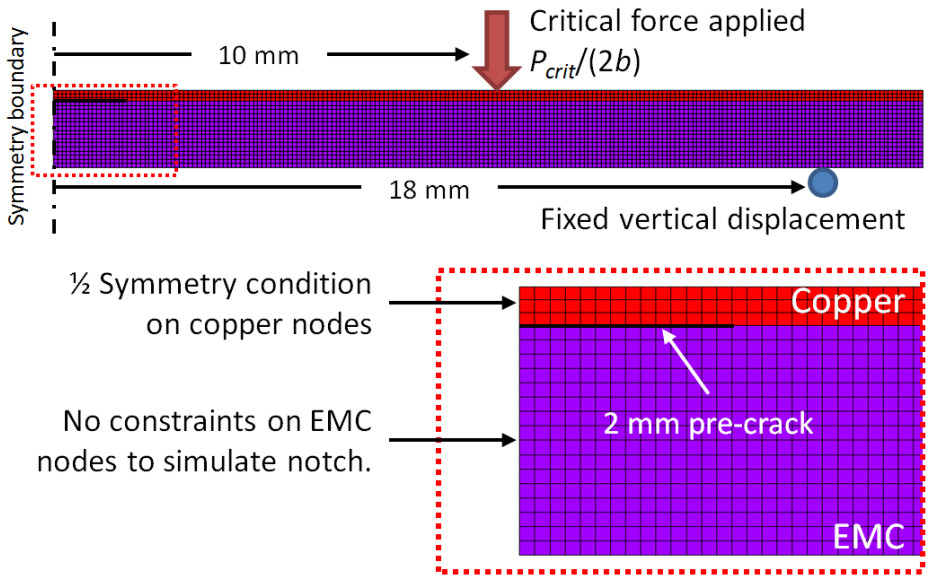

Figure 5.12: 2D model of FPB test.

To reduce computation time, a one-half symmetry model is constructed. Since deformations are small, both copper and EMC are assumed to be linear elastic at room temperature. Material properties from Table 5.1 are used. To capture specimen deformation during delamination propagation, a 2 mm delamination is constructed in the

interface starting from the symmetry line. 2 mm is selected arbitrarily since G is independent of crack length for the FPB test. Copper nodes at the symmetry boundary have displacement constrained in the x-direction. At the narrow support pin, vertical displacement is constrained. At the wide loading pin, a force equivalent to P_{crit} = 6.25 N is applied so that the calculated $G = G_C$. The applied force is the critical force divided by $2b$ to account for symmetry and the specimen width b. The deformed model is shown in Fig. 5.13. Initial simulations do not show crack-interpenetrations and stresses are primarily tensile, so contact pairings are not used in the model.

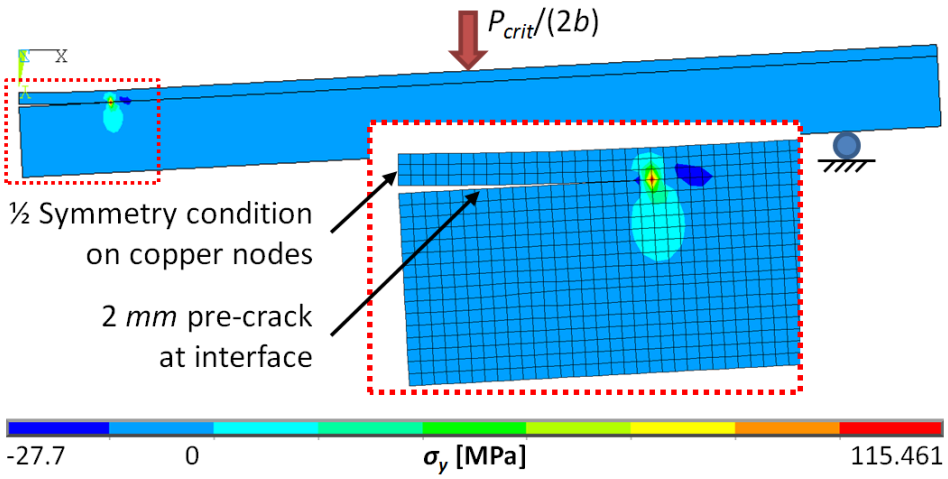

Figure 5.13: Deformed 2D model of FPB test used for calculating G_C and ψ.

The FPB model shows similar stress contours to those at the DCB crack tip. The contours are asymmetric due to the dissimilar layers. The stresses vary with distance and angle from the crack tip. The maximum von mises stress is found to be below the copper yield stress, so the elastic assumption is accepted.

The VCCT method is applied to the deformed model to calculate mode I and mode II energy release rates. From three trials, three measurements are shown in Table 5.3. Using the average P_{crit} of 6.25 N, VCCT returns an average value G_C = 44.6 J/m^2, coincidentally equal to the analytical result.

Table 5.3: G_C calculated for the FPB test.

	P_{crit} [N]	G_C [J/m^2]
Specimen 1	5.946	42.03
Specimen 2	6.305	47.26
Specimen 3	6.491	50.09
Average Force	6.25	44.6

Mode-mixity is obtained through the crack displacement method. From Fig. 5.13, crack displacements are obtained at varying distances from the crack tip. Both sides of (4.11) are plotted in Fig. 5.14. The curves intersect at r = 0.027 mm, so ψ is calculated at this distance from the crack tip. For the FPB test, ψ = 14.0° using (4.10).

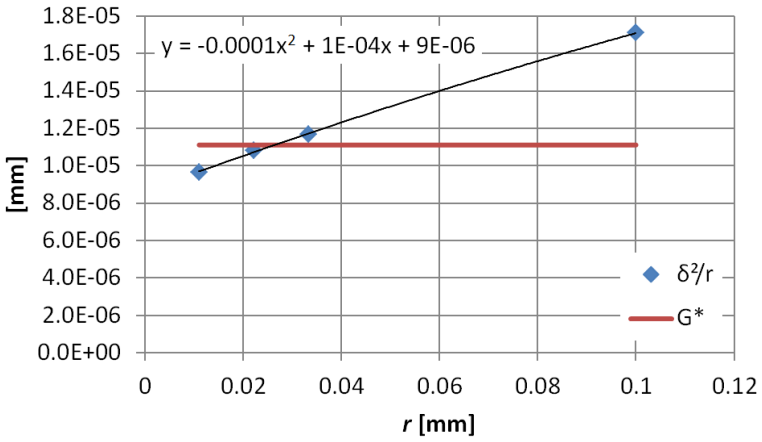

Figure 5.14: Determination of *r* for FPB mode-mixity calculation.

5.3.4 FPB Symmetry Assumption

Analytical and FEM calculations of G_C for the FPB test assume a perfect symmetry in the specimen. This means that delamination initiates in both directions from the EMC notch simultaneously. In reality, the delamination may initiate and propagate in one direction before traveling in the other direction.

Noijen *et al.* investigated the effects of delamination asymmetry on G_C calculations through FEM [50]. They prepared a model displaying one-sided delamination and compared displacements to a fully symmetric model. They determined that differences between symmetric and one-sided delamination are negligible in the steady-state delamination phase. Therefore, symmetry is a valid assumption for analytical calculation of critical strain energy release rate.

5.4 Critical Strain Energy Release Rate Characterization

The results calculated previously are combined to characterize critical strain energy release rate across a range of mode-mixity. G_C versus ψ is plotted in Fig. 5.7. G_C is lowest near mode I loading and G_C increases significantly with ψ. The Hutchinson and Suo model (4.14) is applied to the model to obtain (5.3).

$$G_C = 35.6[1 + \tan^2(0.915\psi)] \tag{5.3}$$

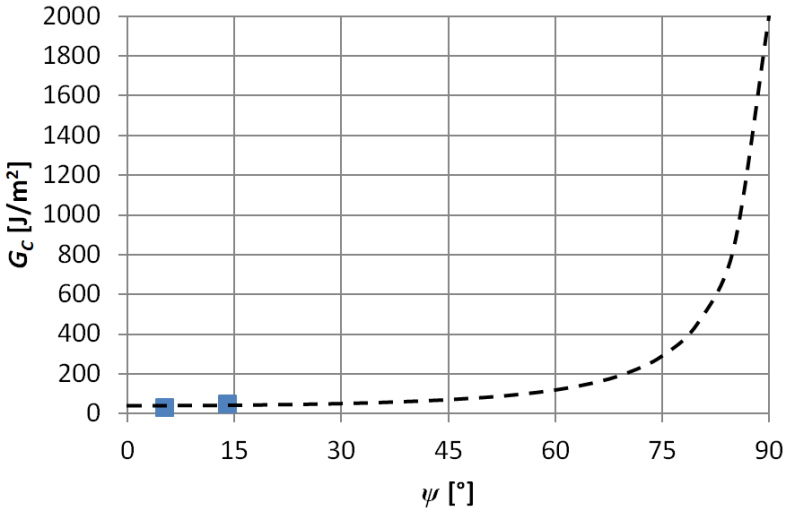

Figure 5.15: G_C versus ψ for the copper/EMC interface.

The model in (5.3) is fitted using the two data points from DCB and FPB results. Since both data points have relatively low mode-mixity, the G_C values at higher mode-mixity are somewhat unknown. Future experiments will need to measure G_C at higher mode mixities and confirm the curve fitted in this work. For this study, the results shown in Fig. 5.15 will be applied in FEM software to develop a mixed-mode cohesive zone model for the copper/EMC interface.

CHAPTER 6

DETERMINATION OF COHESIVE ZONE PARAMETERS

To obtain cohesive zone element properties, both FPB and DCB tests are modeled and simulated with *ANSYS Mechanical APDL*. Since the properties cannot be obtained directly through analytical or numerical results, values will be selected to replicate load-displacement data obtained from experiments.

6.1 Cohesive Zone Model

ANSYS® has built-in CZ elements that may be used to simulate interfacial delamination. For 2D models, six node quadratic CZ elements with plane strain are used. Fig. 6.1 shows the placement of CZ elements along an interface.

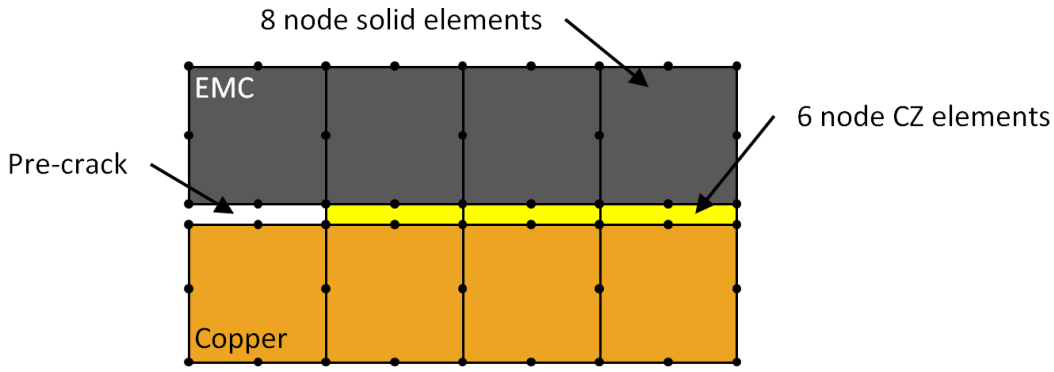

Figure 6.1: Placement of cohesive zone elements at the interface.

Before loading, the elements have zero initial thickness, and nodes from upper and lower surfaces are coincident. A bilinear law is selected to govern interfacial traction

and separation. For the bilinear traction-separation law, six independent parameters are required to fully characterize CZ models for mixed-mode loading conditions. These parameters define two bilinear traction-separation laws corresponding to pure mode I and pure mode II delamination.

6.2 DCB Cohesive Zone Modeling

Since DCB loading of a bimaterial specimen is close to pure mode I loading, a CZ model of the DCB test will be prepared first. The DCB cohesive zone model appears in Fig. 6.2.

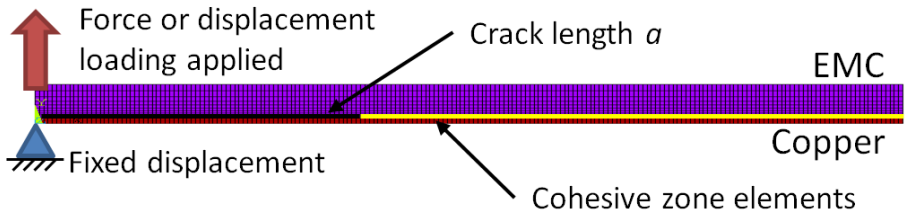

Figure 6.2: 2D cohesive zone model of DCB test.

The DCB experiment is modeled using 2D elements with plane strain. Eight node quadratic elements are used for copper and EMC layers, and six node quadratic CZ elements are inserted along the interface. An initial crack with pre-set length is placed at the left end of the specimen. Within the crack, no CZ elements are inserted and nodes are left uncoupled so that there are no interactions between surfaces. At the left end of the specimen, one copper node at the bottom surface is fixed in both vertical and horizontal directions. One EMC node at the upper surface is used to apply variable displacement loading. Plasticity is again assumed to be negligible for small deformations, and linear

elastic material models are used for copper and EMC. Material properties from Table 5.1 are used. Based on results from previous simulations, no contact pairings are used in the model.

6.3 FPB Cohesive Zone Modeling

A FPB cohesive model of the specimen is also prepared. The CZ model also takes advantage of one-half symmetry to reduce computation time. The FPB cohesive zone model is shown in Fig. 6.3.

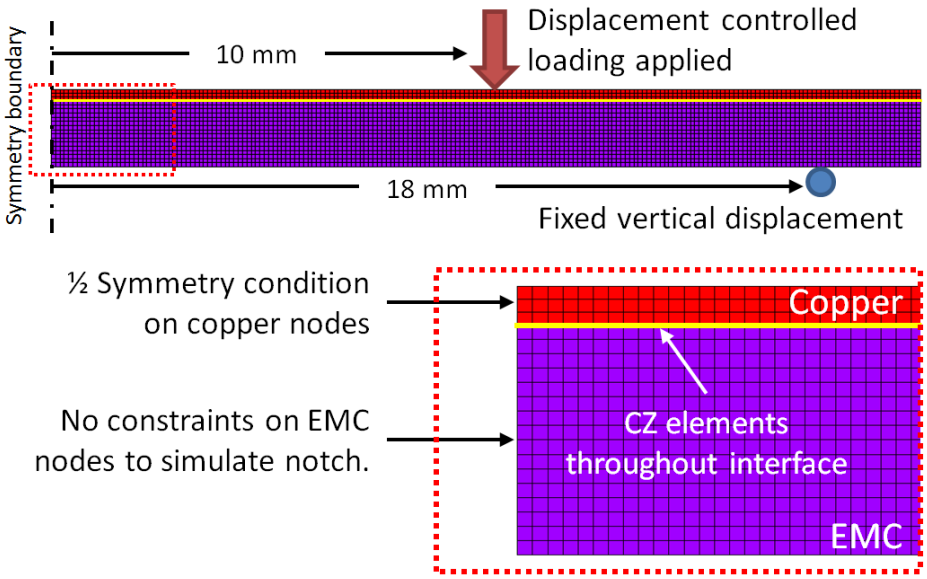

Figure 6.3: 2D cohesive zone model of FPB test.

The FPB experiment is modeled using 2D elements with plane strain. Eight node quadratic elements are again used for bimaterial layers, and six node quadratic CZ elements are inserted between copper and EMC. No initial crack is constructed; CZ elements are placed throughout the length of the specimen. To simulate the EMC notch,

a symmetry boundary condition is applied only to the copper layer so that the left face of the EMC layer is unconstrained. Plasticity is neglected and linear elastic material models are again used with material properties from Table 5.1. Based on results from previous simulations, no contact pairings are included in the model.

6.4 Simulated Load-Displacement Results

Using the DCB and FPB cohesive zone models, displacement controlled loading is applied to simulate the experimental results. The cohesive zone parameters are selected so that simulated data matches the experimental data

A general design procedure for determining cohesive zone properties for the bilinear traction-separation law is as follows. First, the mode I bilinear law is considered. The area of the triangle is set to G_C for mode I from Fig. 5.15. σ_{max} is adjusted to cause delamination at the appropriate critical force. α can be modified to fine-tune the initial slope and shape of the load-displacement response. For the mode II bilinear law, the area of the triangle is set to G_C for mode II from Fig. 5.15. After several iterations, the mixed-mode CZ model is used to simulate the following results.

6.4.1 Double Cantilever Beam Simulation

Using the mixed-mode CZ model for copper/EMC interface, a DCB load-displacement response is simulated for different crack lengths and plotted against data from experiments (Fig. 6.4, 6.5).

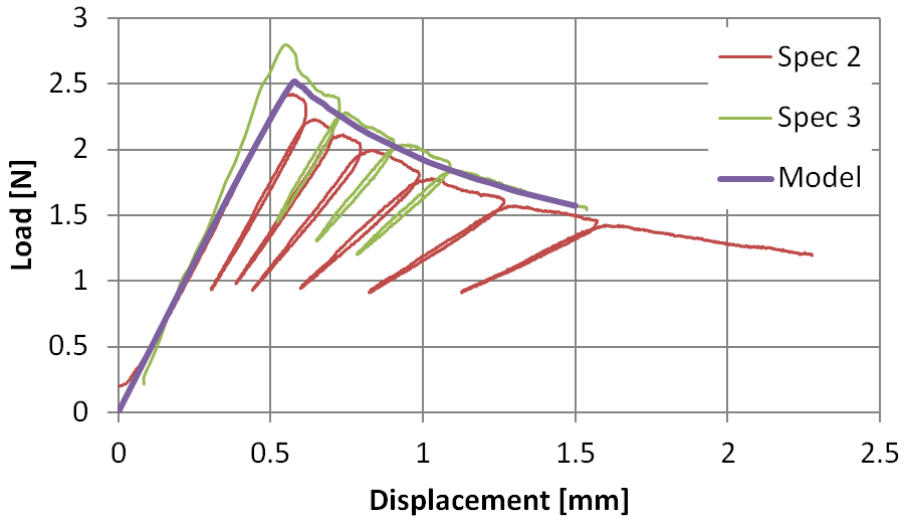

Figure 6.4: Simulated DCB load-displacement data with 9 mm starter crack using cohesive zone modeling.

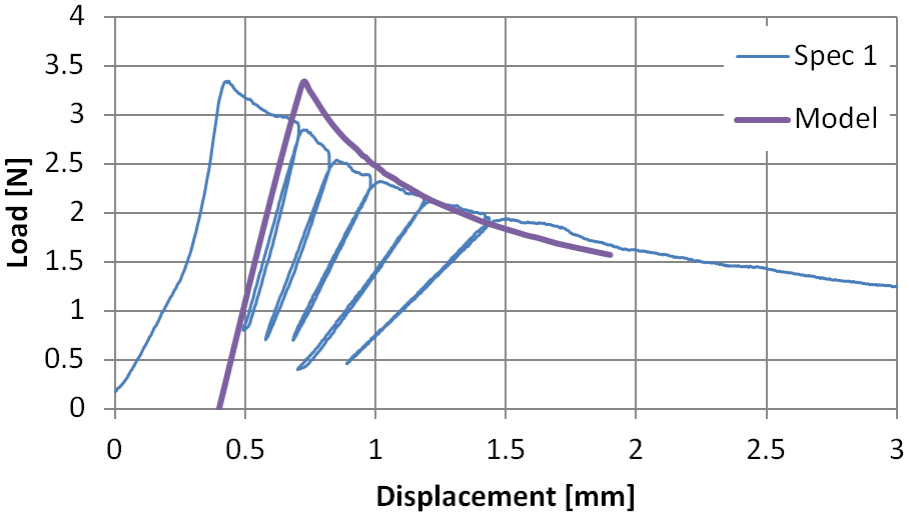

Figure 6.5: Simulated DCB load-displacement data with 6.35 mm starter crack using cohesive zone modeling.

Since compliance varies with crack length, the initial slope and peak force are controlled by the pre-set starter crack length. For crack lengths of 9 mm and 6.35 mm, the CZ model is able to capture the experimental behavior. After an initial peak load, the

model shows reduction in load, indicating interfacial delamination in the CZ elements. The load continues to drop as displacement increases.

6.4.2 Four-point Bend Simulation

Using the same mixed-mode CZ model, the FPB load-displacement response is simulated and plotted against experimental results in Fig. 6.6.

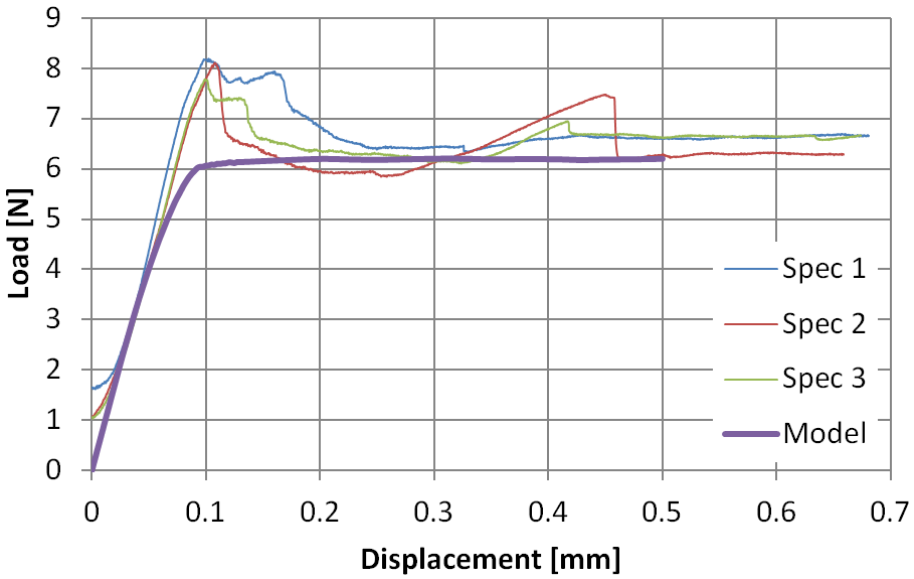

Figure 6.6: Simulated FPB load-displacement data using cohesive zone modeling.

Crack propagation through the molding compound is not simulated, so the model does not capture the initial peak loads seen in experiments. The model captures the initial specimen stiffness and the constant force P_{crit} for steady-state delamination.

6.5 Cohesive Zone Parameters

Thus, the selected cohesive zone parameters are capable of replicating mixed-mode delamination for the FPB test and DCB test. Load-displacement data captures

critical forces and displacements for delamination as well as initial loading stiffness behavior. The mixed-mode bilinear law is shown in Fig. 6.7, with all six parameters listed in Table 6.1. The fully-defined cohesive zone model may be used to simulate mixed-mode interfacial delamination between copper leadframe and epoxy molding compound in any geometry.

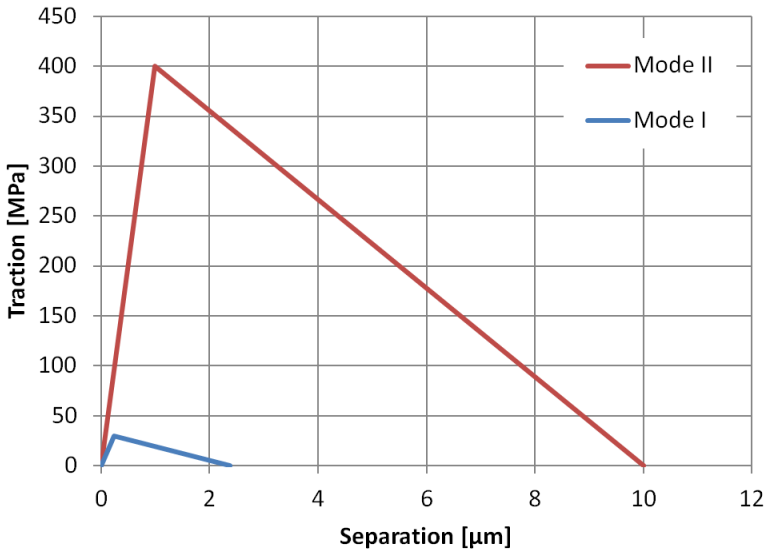

Figure 6.7: Mixed-mode bilinear traction-separation law for the copper/EMC interface.

Table 6.1: Mixed-mode cohesive zone parameters for the copper/EMC interface.

	Mode I	**Mode II**
σ_{max} **[MPa]**	30	400
δ_C **[μm]**	2.373	10
δ^* **[μm]**	0.2373	1

CHAPTER 7

COPPER/EMC DELAMINATION IN SOIC PACKAGE

Cohesive zone parameters have been determined as a more powerful tool for investigating interfacial delamination between copper and EMC in microelectronic packaging. To demonstrate the use of the mixed-mode CZ model, a small outline integrate circuit (SOIC) package is examined.

In SOIC fabrication, EMC is dispensed by the same transfer molding process used to prepare the bimaterial specimens. Identical EMC/copper materials and cure temperatures are used with similar moisture and surface roughness conditions. Therefore the experimental results measured with the bimaterial specimens are expected to provide a good representation of the interface within the SOIC package. Thus, both G_C measurements and cohesive zone parameters apply to behavior of the copper/EMC interface in the SOIC package.

First, a stress-based analysis of the SOIC package is completed to verify the location of the critical region. A fracture mechanics approach is used to evaluate SERR along the critical interface, and results are compared the experimental results. Finally, cohesive zone elements are placed along the interface to determine if the interface will fail. Using the CZ model, design guidelines for SOIC packaging are obtained through a parametric study.

The SOIC package is a common package used in microelectronic design due to inexpensive and simple fabrication processes. The SOIC package has five key

components: copper leadframe, silicon die, die attach, wire bond, and molding compound (Fig. 7.1).

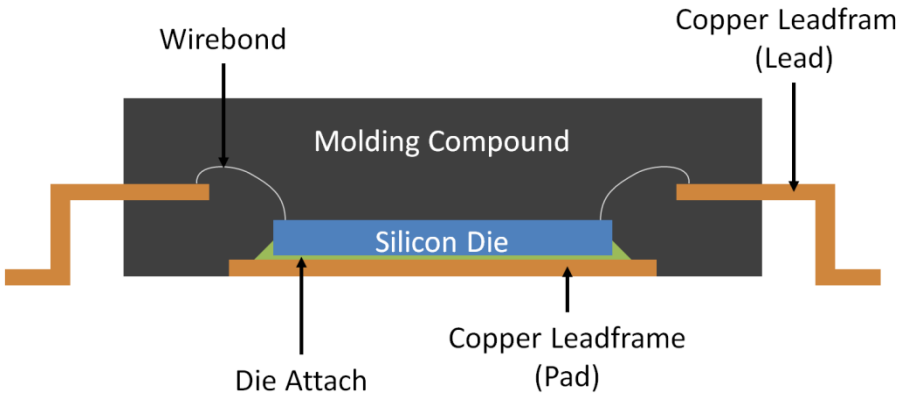

Figure 7.1: 2D cross-section of SOIC package geometry.

The copper leadframe forms the foundation of the SOIC package. The leadframe holds all functional components of the package and provides interconnections to the system board. The silicon die is attached to the leadframe with a die attach adhesive. To complete the interconnections, wire bonds are formed from the die to the leadframe. An epoxy molding compound (EMC) is applied over the entire package to encapsulate and protect the die and wire bonds. Copper leads extend outside the molding compound to form board-level interconnections.

At either end of the copper pad, EMC is bonded directly to the copper leadframe. This interface has been identified as a critical failure location for SOIC packages. The critical interface is shown in Fig. 7.2. On the right side of the interface, the copper pad is bounded by EMC. On the left, a trimaterial boundary is formed where EMC, copper pad,

and die attach meet. High stresses are expected to develop along the copper/EMC interface due to mismatch in CTE between these materials.

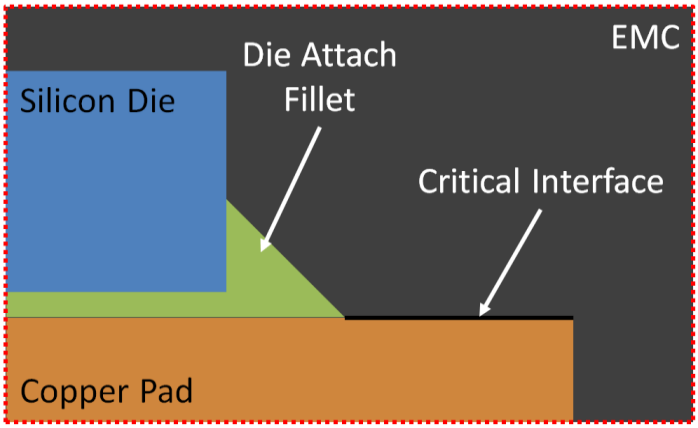

Figure 7.2: The critical copper/EMC interface located at the exposed copper pad.

Fabrication of the SOIC package requires two thermal excursions, outlined in Fig. 7.3. The leadframe shape is stamped from a copper sheet. Liquid die attach adhesive is dispensed, then the die is attached and the adhesive is cured at 225 °C. The package is cooled to room temperature, and electrical connections to copper leads are formed via wire bonding. Lastly, the package is pre-heated, and a liquid epoxy molding compound is injected into a mold. The EMC cures at 175 °C, then the completed package is cooled to room temperature and ejected from the mold.

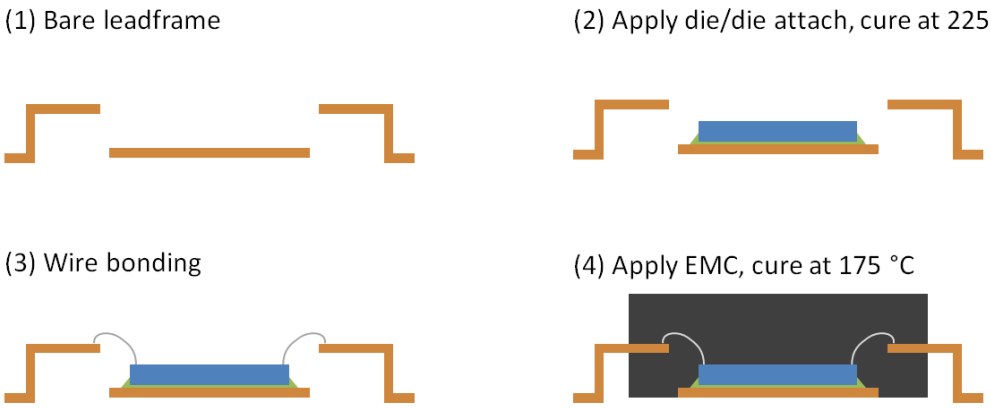

Figure 7.3: SOIC fabrication process.

7.1 Package Geometry and Boundary Conditions

To save computation time, a half symmetry model is constructed as shown in Fig. 7.4. Typical SOIC geometry is obtained from component datasheets.

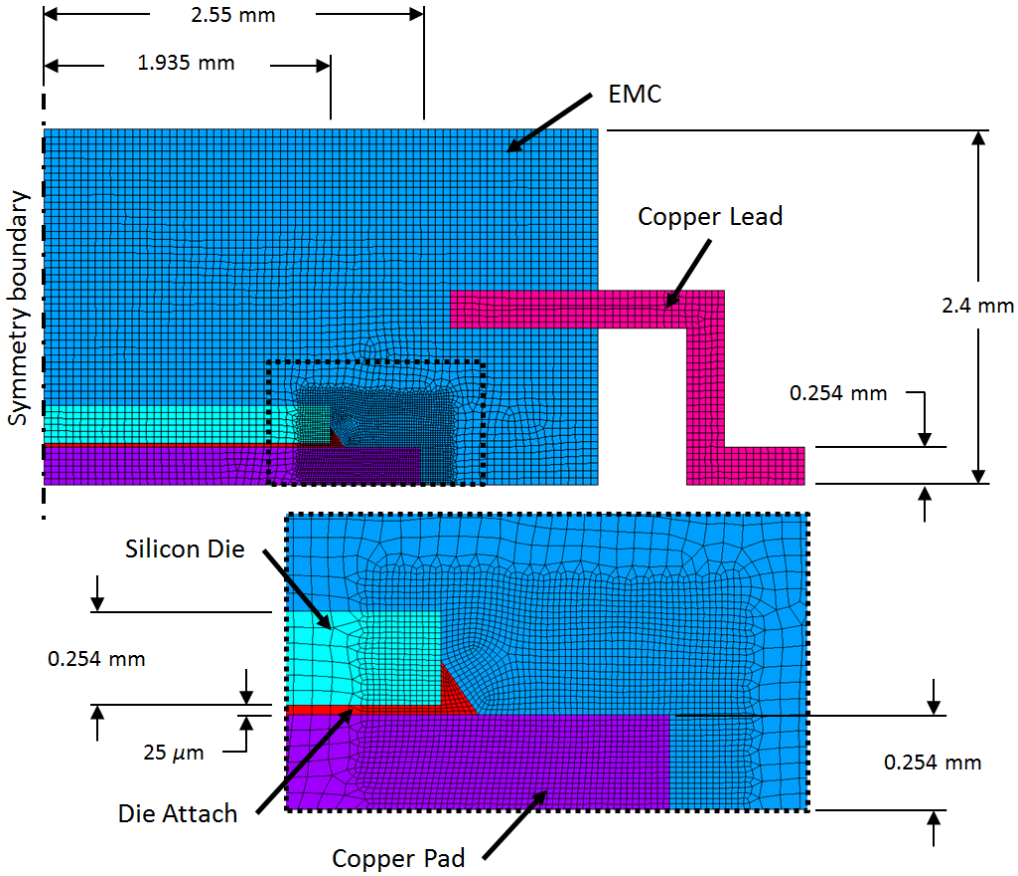

Figure 7.4: 2D model of SOIC package.

The die is attached to the copper pad by a single layer of die attach elements. The die attach fillet is modeled since it is expected to have a significant effect on stresses in the critical region. The die/copper pad assembly is encapsulated by the epoxy molding compound, and the copper lead extends from the package. Wire bonds have extremely low stiffness and are not expected to contribute to package stresses, so they are omitted from the model.

At the left edge of the model, all nodes are constrained in the horizontal direction to create the symmetry boundary condition. Additionally, one node is constrained in the

vertical direction to prevent rigid body motion. Thermo-mechanical loading is applied via a uniform temperature on all nodes.

7.2 Material Models

In the SOIC package, stresses are developed from CTE mismatch under thermal loading. Thus, temperature dependent properties must be incorporated wherever applicable. The following material properties have been obtained from literature and industry for modeling microelectronic packaging. Stress-free reference temperatures T_{ref} are selected based on fabrication processes discussed in section 7.3.

7.2.1 Copper Leadframe

For the leadframe material, CDA194 high strength modified copper is used. The material has excellent workability for forming into the leadframe shape and excellent corrosion resistance and electrical properties. A linear elastic material model is selected, since stresses are not expected to approach the yield stress. Material properties in Table 7.1 are obtained from material datasheets. The pad begins to develop stresses as the package cools from the die attach cure temperature, so the reference temperature is selected to be the die attach cure temperature. The lead does not come into contact with the die or die attach before EMC is applied, so no stresses are incurred until then. The reference temperature for the lead is chosen to be the EMC cure temperature.

Table 7.1: Copper leadframe material properties.

Property	Value
E [GPa]	121
v	0.35
α [ppm/°C]	17.6
T_{ref} [°C]	225 (pad) 175 (lead)

7.2.2 Silicon Die

For modeling silicon dies in microelectronic packaging, anisotropy is not prominent and an isotropic model can be used [21]. Therefore, the die is modeled as a linear elastic, isotropic material. Material properties have been obtained from literature [21]. The reference temperature is selected to be the die attach cure temperature.

Table 7.2: Silicon die material properties.

Property	Value
E [GPa]	170
v	0.30
α [ppm/°C]	2.33
T_{ref} [°C]	225

7.2.3 Die Attach Adhesive

The silicon die is attached to the leadframe by a *DIEMAT DM4130HT/J154-5* thermoplastic/thermoset adhesive paste. The adhesive is a very thin layer with very low stiffness compared to other materials. Therefore, a linear elastic temperature independent model is used. Material properties are obtained from material datasheets, and the reference temperature is set to the cure temperature.

Table 7.3: Die attach adhesive material properties.

Property	Value
E [GPa]	2.3
v	0.35
α [ppm/°C]	32
T_{ref} [°C]	225

7.2.4 Epoxy Molding Compound

To encapsulate and protect the die and wire bonds, a *SUMITOMO BAKELITE SUMIKON® EME-G630AY* epoxy molding compound is used. EMC stiffness is heavily dependent on temperature, so stiffness and CTE values are applied above and below the glass transition temperature 140 °C. For this analysis, a linear thermo-elastic formulation is assumed valid. Material properties are obtained from material datasheets.

As the EMC cures and solidifies, some shrinkage occurs in the molding compound that is unrelated to CTE. This behavior is known as cure shrinkage. The SOIC model should account for cure shrinkage to accurately capture thermo-mechanical stresses in the package. A study on cure shrinkage in EMC materials found a typical 1% volumetric shrinkage during cure [51]. Thus cure shrinkage in the EMC can be accounted for by increasing the simulated reference temperature to account for the 1% volumetric shrinkage as shown in (7.1).

$$T'_{ref} = T_{ref} + \frac{0.1\%}{3\alpha} \tag{7.1}$$

Applying this formula, the EMC cure temperature of 175 °C produces a reference temperature of 185.42 °C.

Table 7.4: Epoxy molding compound material properties.

Property	Value
E [GPa]	25 at 25 °C 0.7 at 260 °C
v	0.30
α [ppm/°C]	9 at 25 °C 32 at 260 °C
T_{ref} [°C]	185.42

7.3 Process Modeling

To simulate stresses incurred from fabricating the package, process modeling is applied to the model. With process modeling, several thermal loads are applied to the model to simulate the excursions required to create the package. In addition, element birth and death is used to introduce package components at the correct stages of assembly.

Element birth and death is a common FEM technique for simulating sequential assemblies. Using element birth and death, elements are created in a killed state, in which the stiffness is reduced by several orders of magnitude, and the element develops no stresses. Elements are birthed at the appropriate step of fabrication and at the stress-free cure or bonding temperature. Birthing an element returns its original material properties.

The FEM process model is based on the fabrication outlined in Fig. 7.3. In an SOIC fabrication, the die is first bonded to the copper leadframe using the die attach epoxy. The epoxy is applied and cured at a high temperature, and then the package is cooled to room temperature. Second, epoxy molding compound is dispensed and cured

at a high temperature, and then the package is once again cooled to room temperature, completing the assembly process. Therefore, process modeling is utilized in *ANSYS* with the following routine in Table 7.5. Room temperature is assumed to be 25 °C.

Table 7.5: Process modeling for SOIC package assembly.

Load Step	Live Components	Description
1	Copper pad	Heat copper pad to 225°C
2	Copper pad, silicon die, die attach	Attach die and cool to 25 °C
3	Copper pad, silicon die, die attach	Heat die/leadframe to 175 °C
4	All components	Cool package to 25 °C

7.4 Stress Contours in SOIC Package

After completing the process modeling in Table 7.5, the package incurs the following normal and shear stress contours, in units of MPa.

Figure 7.5: Normal stress σ_y [MPa] in the SOIC package after process modeling.

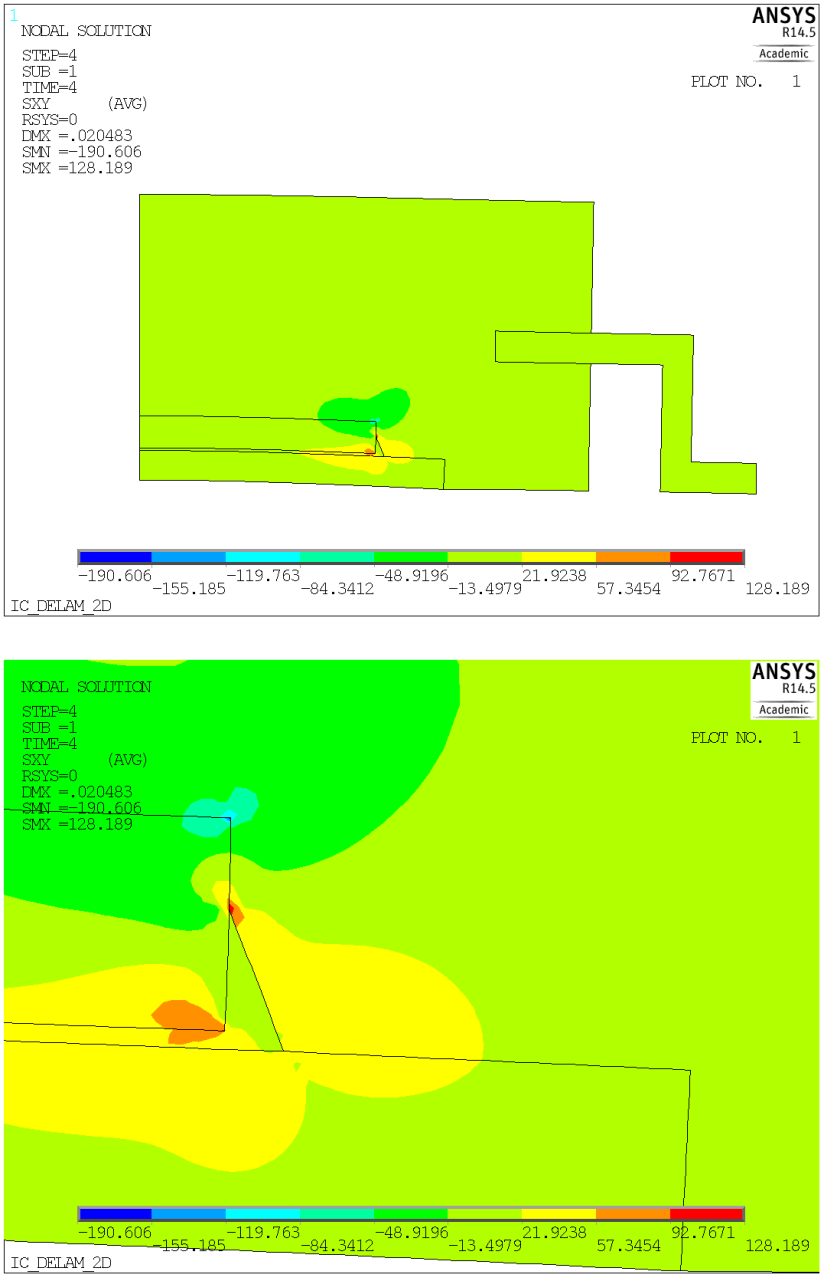

Figure 7.6: Shear stress σ_{xy} [MPa] in the SOIC package after process modeling.

After cooling to room temperature, the package is in a generally compressive stress-state. In the copper lead and most of the molding compound, both normal and shear stresses are minimal. Both normal and shear stress contours show elevated values

along the critical interface between copper and mold compound. From Fig. 7.5, normal stresses are generally compressive, though tensile stresses are found at either end of the interface. Normal stresses are especially high on the left side, at the tip of the die attach. Similarly, shear stresses show much higher values at this interface. Therefore, the left side of the interface is a likely starting location for an interfacial crack between copper and EMC. Normal and shear stresses along the interface are plotted along the interface in Fig. 7.7, where a coordinate of zero signifies the left side of the interface.

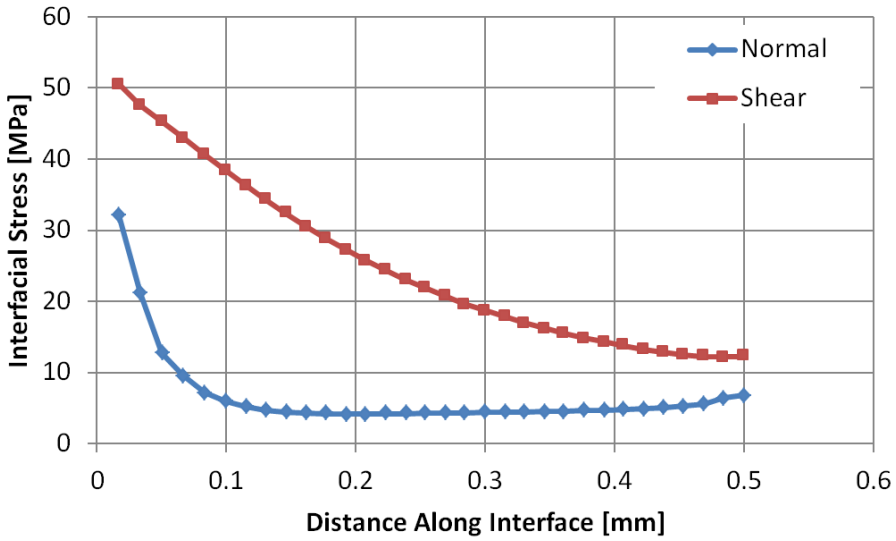

Figure 7.7: Stresses along the copper/EMC interface after process modeling.

7.5 Interfacial Fracture Mechanics Analysis

Before cohesive zone elements are inserted along the interface, an initial fracture mechanics analysis is performed on the copper/EMC interface. After process modeling, stress contours suggest that the left side of the interface is a likely starting location for an interfacial crack. Using the SOIC model shown in Fig. 7.4, a starter crack is inserted

along the interface by leaving several nodes uncoupled beginning from the left side of the critical interface. The starter crack location is shown in Fig. 7.8.

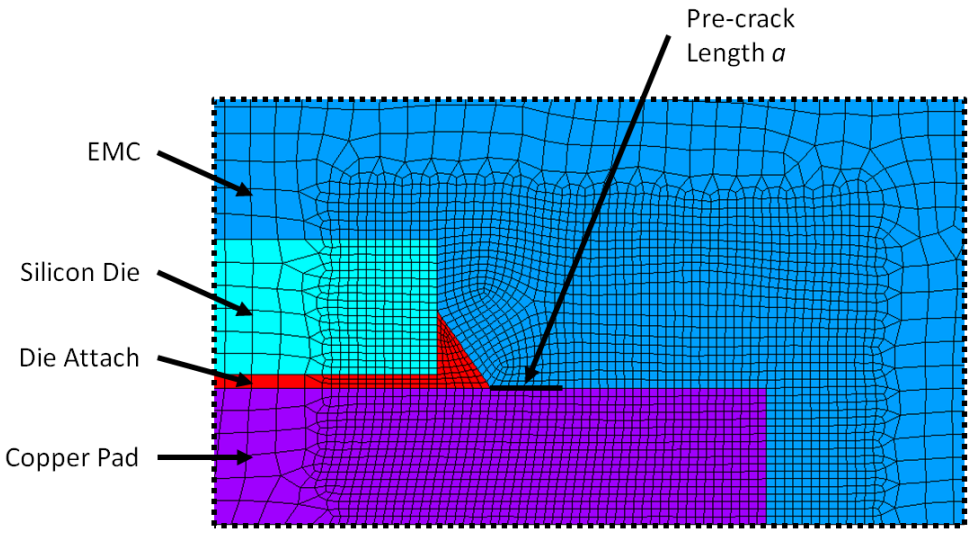

Figure 7.8: Pre-crack inserted into the 2D SOIC model.

After the starter crack is built, process modeling is again applied to the model. Nodes along the interface are coupled until the final loading step when the completed package is cooled to room temperature. An initial simulation of process modeling showed some inter-penetration of crack surfaces. To prevent this, a surface-to-surface contact pairing is applied to nodes in the pre-crack, and the simulation is repeated. Contact surfaces are assumed frictionless. The deformed crack shape for a starter crack of length 0.1 mm is shown in Fig. 7.9.

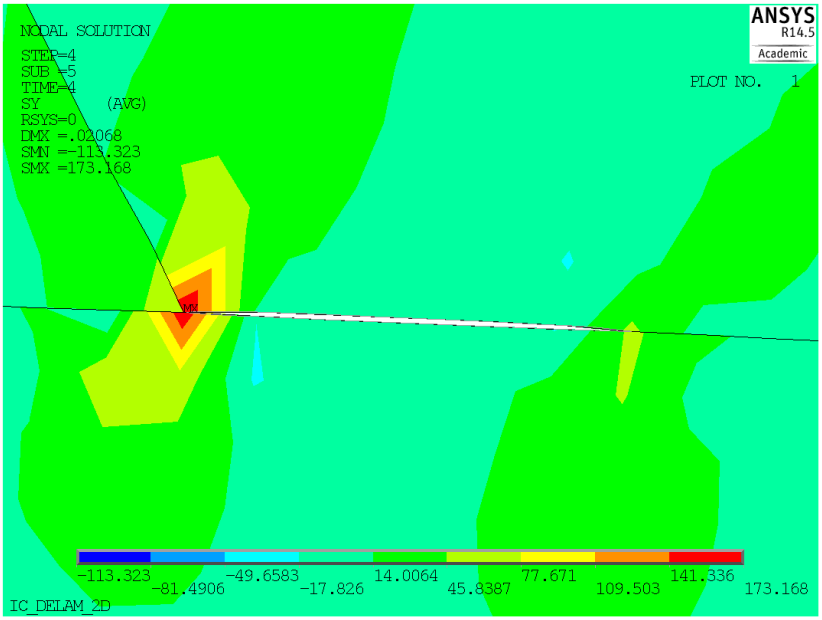

Figure 7.9: Normal stress σ_y [MPa] near the pre-crack in the SOIC after process modeling

Using VCCT, *G* is calculated at the copper/EMC crack tip for varying pre-crack length *a*. Results are shown in Fig. 7.10.

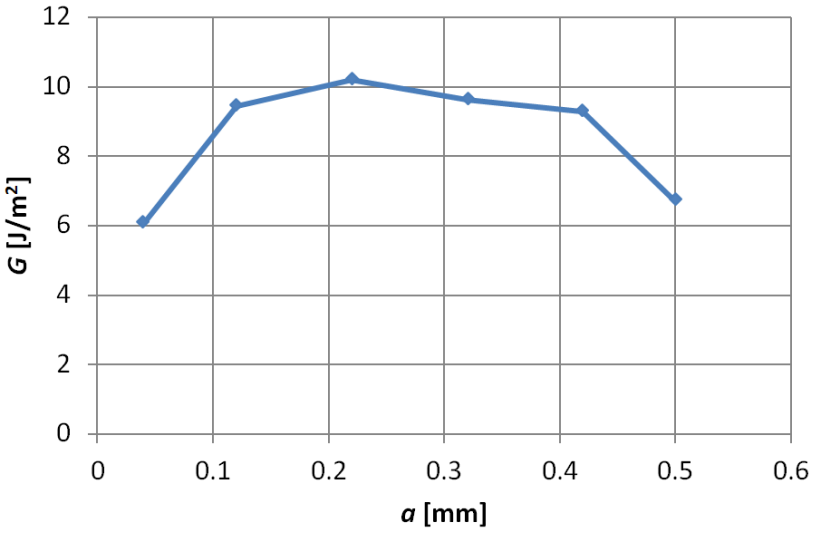

Figure 7.10: SERR at the copper/EMC crack tip versus crack length.

At all crack lengths, SERR is far below the critical SERR determined through experiments. Therefore, fracture mechanics predicts that no delamination will occur after fabrication processes.

7.6 Cohesive Zone Delamination Analysis

Now the model shown in Fig. 7.4 is rebuilt using cohesive zone elements. Cohesive zone elements are placed along the copper/EMC interface in the critical region as shown in Fig. 7.11.

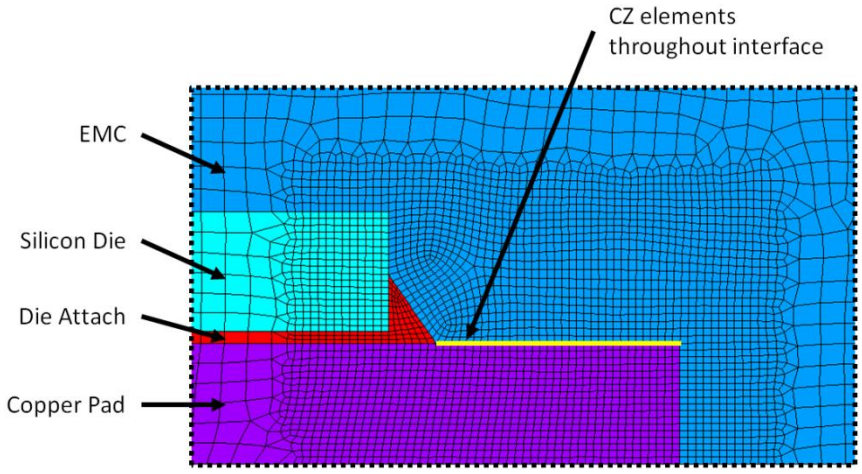

Figure 7.11: Cohesive zone elements inserted into the 2D SOIC model.

Process modeling is again applied to the cohesive zone model. Nodes along the interface are coupled until the final loading step to prevent separation before the EMC has been activated. A frictionless surface-to-surface contact pairing is applied to nodes at the interface to prevent crack surface inter-penetration. Fig. 7.12 and Fig. 7.13 show normal and shear stress contours in the package.

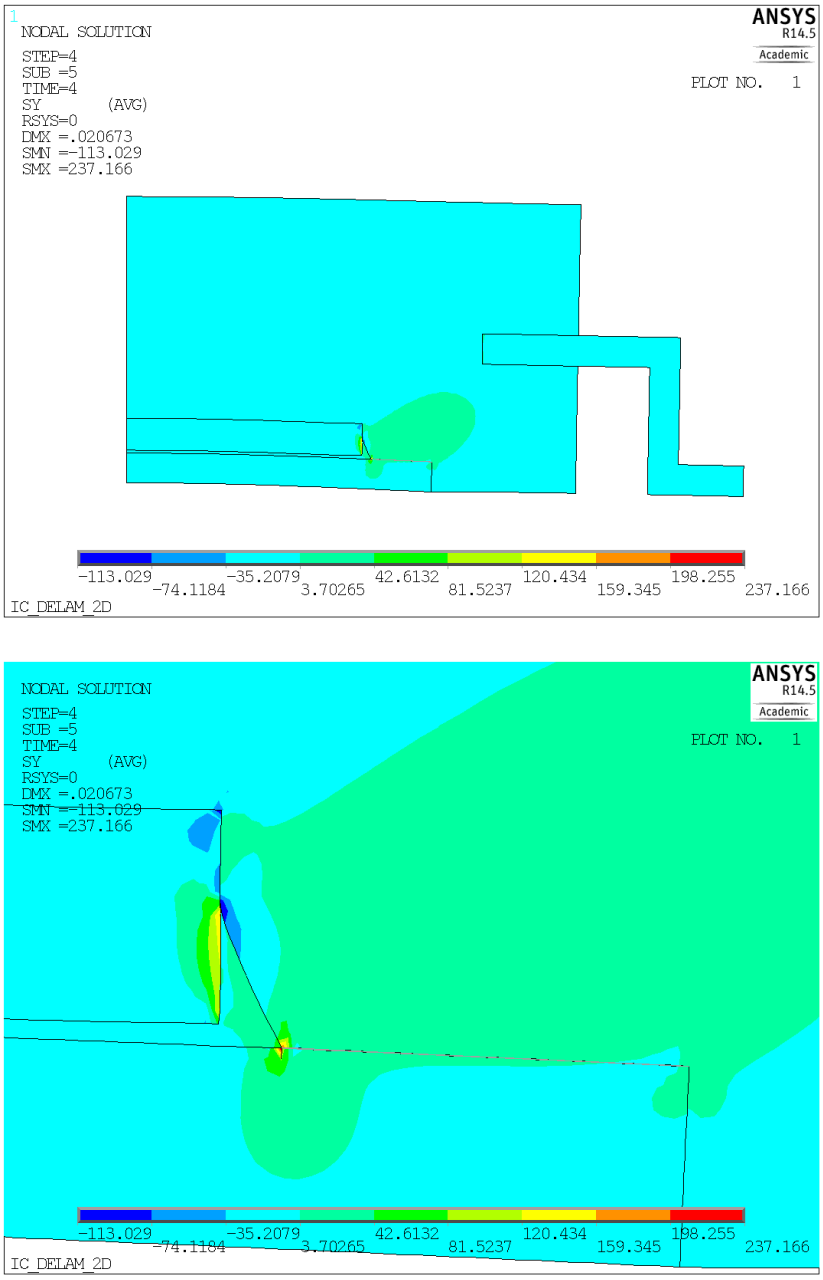

Figure 7.12: Normal stress σ_y [MPa] in the SOIC package after process modeling with CZ elements.

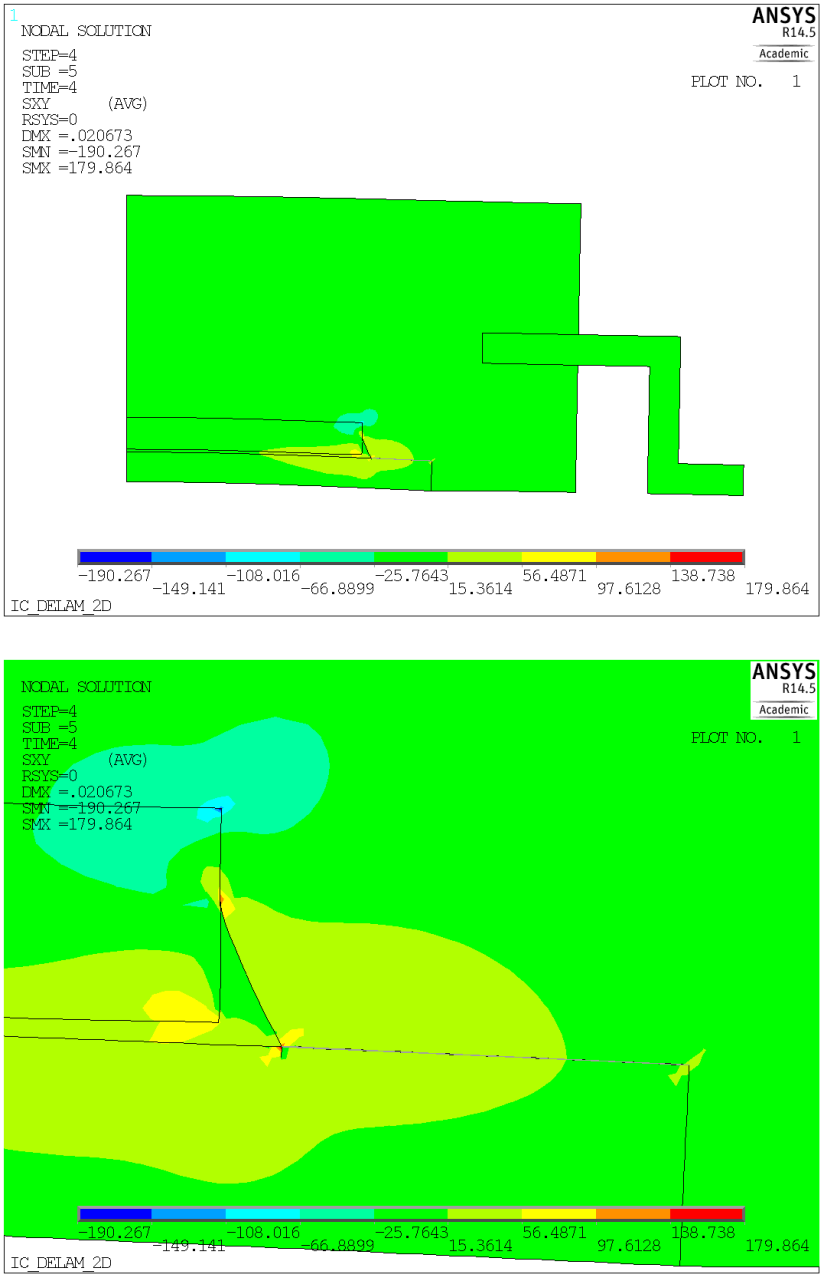

Figure 7.13: Shear stress σ_{xy} [MPa] in the SOIC package after process modeling with CZ elements.

Interfacial separation is plotted along the interface in Fig. 7.14, where distance along the interface is again measured from the left side. For both normal and shear separation, $\delta(x) < \delta^*$ and therefore the damage in the interface is zero.

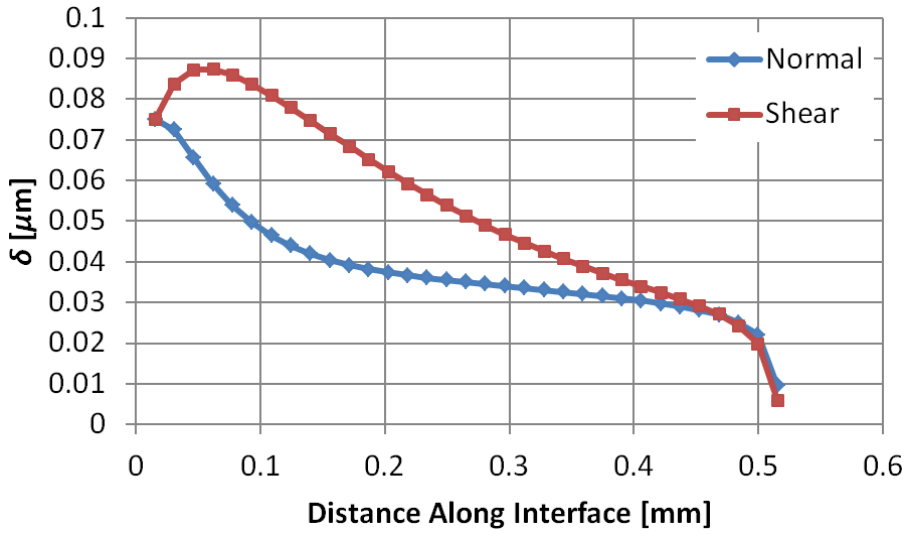

Figure 7.14: Interfacial separation in CZ elements after process modeling.

Since the entire interface is undamaged, the interface is fully closed. The cohesive zone results are compared to the closed-crack model (Fig. 7.7). Fig. 7.15 shows closed-crack interfacial stresses and cohesive zone interfacial stresses. The cohesive zone model is able to capture the closed-crack stress contours along the interface.

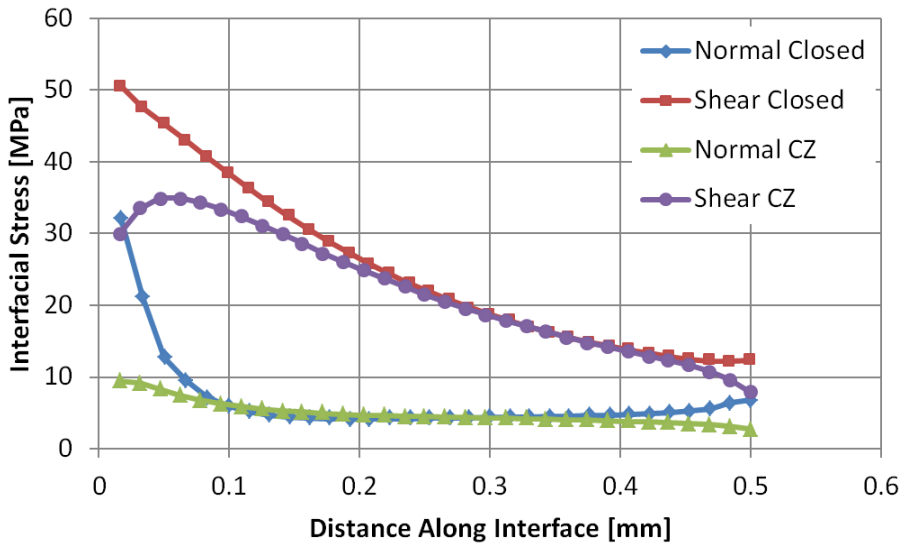

Figure 7.15: Interfacial stresses simulated by closed-crack and cohesive zone models.

7.7 Parametric Study of Geometric Parameters

Now that the predictive SOIC model has been created, several geometric parameters are varied and simulated using cohesive zone elements at the interface. Interfacial separation is plotted for several different parameters in the following figures. These plots are used to develop geometric design guidelines for SOIC packages. For simplicity, normal interfacial separations are plotted for various geometric parameters. The effects of die thickness, interfacial length, EMC thickness, die attach cure temperature, and EMC cure temperature are examined. In the following figures, blue coloring indicates nominal parameters used in Fig. 7.13. All other dimensions and parameters are kept at the nominal value when possible.

The die subassembly goes through two thermal excursions and is expected to contribute significantly to interfacial separation. In the SOIC model, die thickness is modeled at 0.254 mm, 0.5 mm, 0.75 mm.

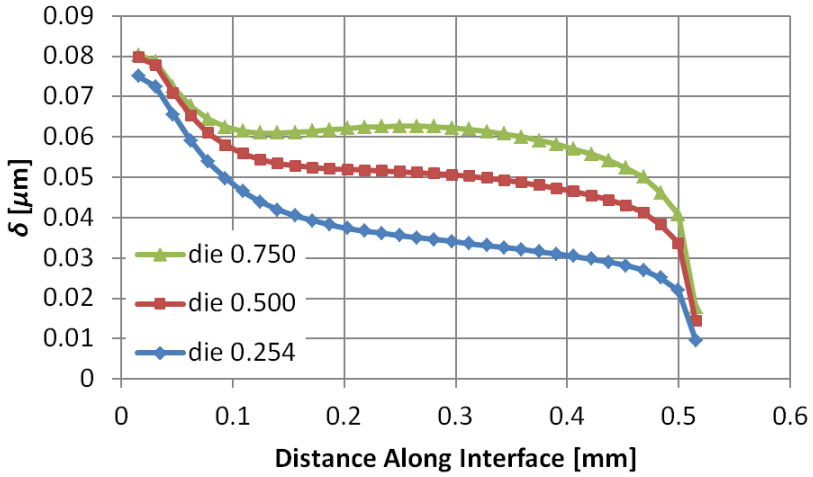

Figure 7.16: Normal separation with varying die thickness [mm].

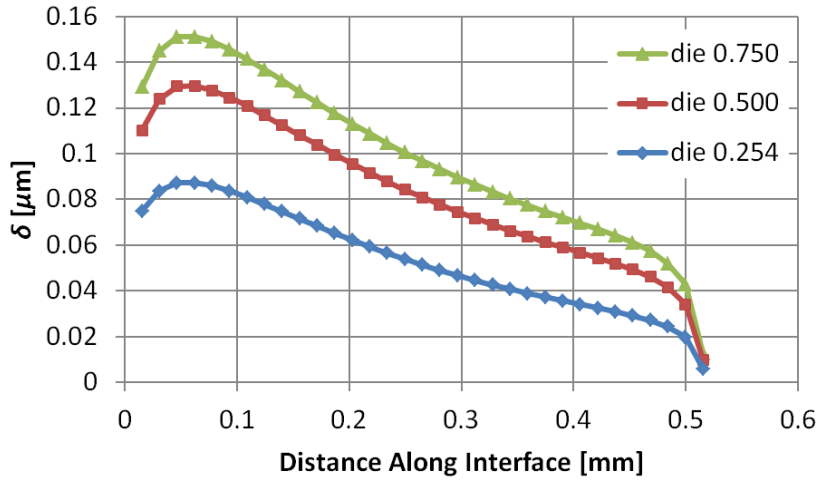

Figure 7.17: Shear separation with varying die thickness [mm].

As expected, increasing the die thickness increases the damage in the interface. Silicon has low CTE compared to copper. This causes high shear stresses to the right of the die. A thinner die will help reduce the likelihood of interfacial delamination in the SOIC package.

If the die area changes, the interface can become much shorter or longer. In the model, die width is modified so that the interface is simulated at lengths of 0.515 mm, 0.980 mm, and 0.35 mm.

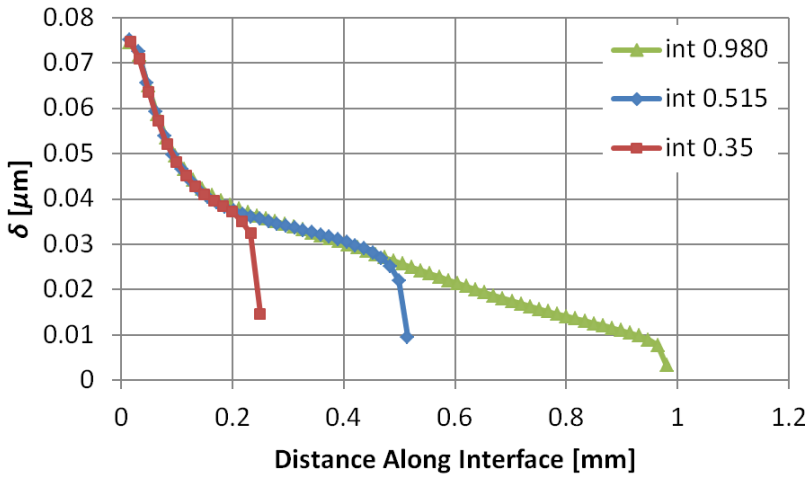

Figure 7.18: Normal separation with varying interface length [mm].

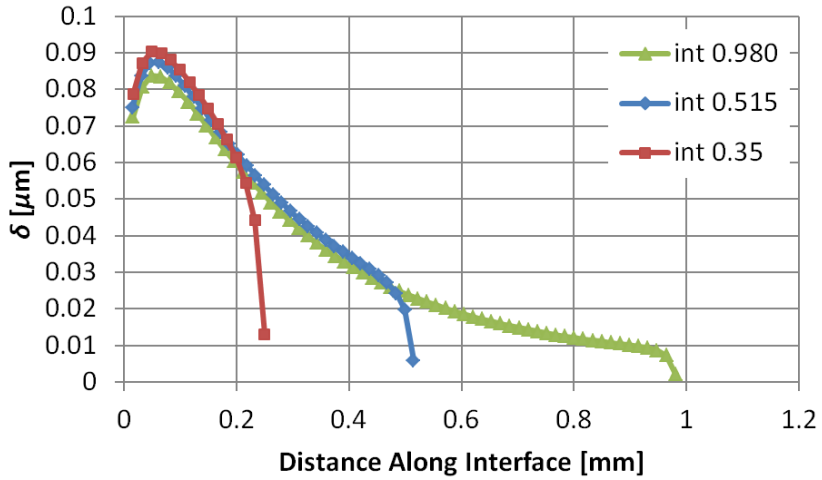

Figure 7.19: Shear separation with varying interface length [mm].

The length of the interface does not have much effect on the interfacial separation near the left side of the interface. However, as the distance along the interface increases, δ continues to decrease. Therefore, in a longer interface, there is more chance that a propagating crack will arrest before reaching the right side of the copper pad.

If the overall package thickness is reduced, the EMC height above the die is reduced. EMC thicknesses of 1.867 mm, 1.667 mm, and 1.467 mm are modeled, measured from the upper surface of the die. From the following figures, changing the EMC thickness has no significant effect on interfacial separation.

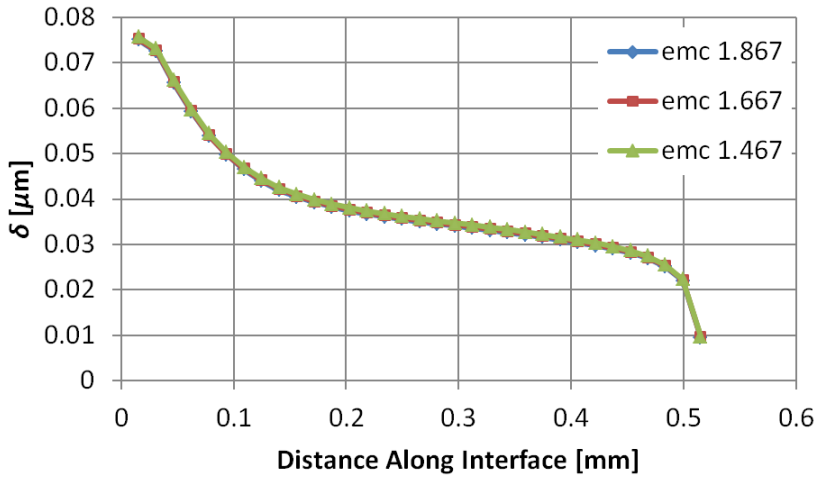

Figure 7.20: Normal separation with varying EMC thickness above die [mm].

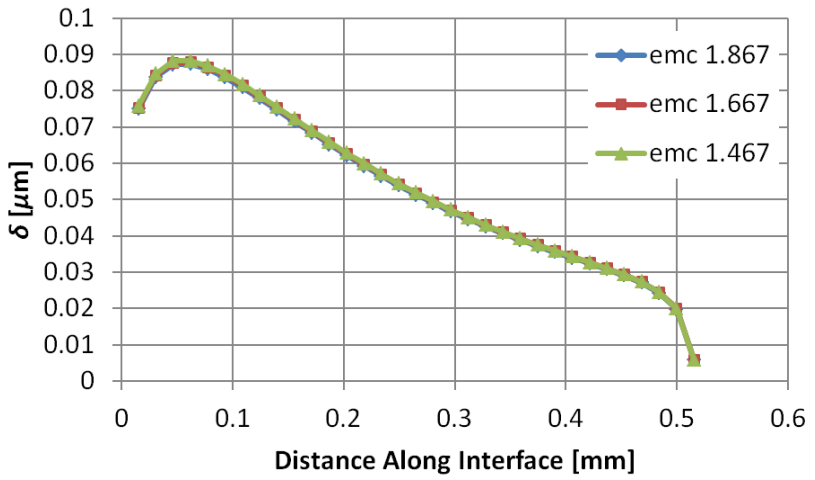

Figure 7.21: Shear separation with varying EMC thickness above die [mm].

Several products are available for attaching the die to the copper leadframe. Material properties may be similar, but different curing temperatures may be required. The SOIC package is modeled with die attach cure temperatures of 225 °C, 245 °C, and 205 °C. Material reference temperatures are modified where appropriate.

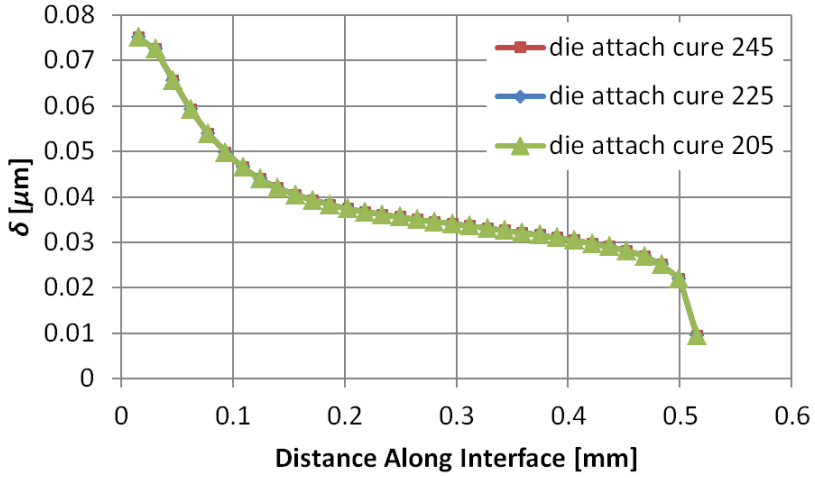

Figure 7.22: Normal separation with varying die attach cure temperature [°].

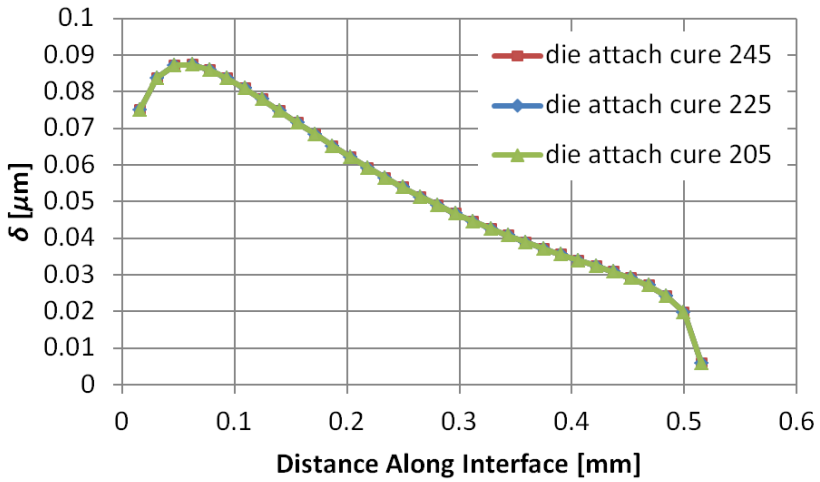

Figure 7.23: Shear separation with varying die attach cure temperature [°].

Since the EMC material is not active when the die is attached, the die attach cure temperature has no effect on the interfacial separation. Therefore the die attach material does not contribute to copper/EMC interfacial delamination.

Similarly, various EMC materials require different cure temperatures. Interfacial stresses are incurred during the final cooling to room temperature, so EMC cure temperature should have a significant effect on interfacial separation. Temperatures of 175 °C, 195 °C, and 155 °C are modeled. In each simulation, the cure shrinkage consideration for the EMC is updated.

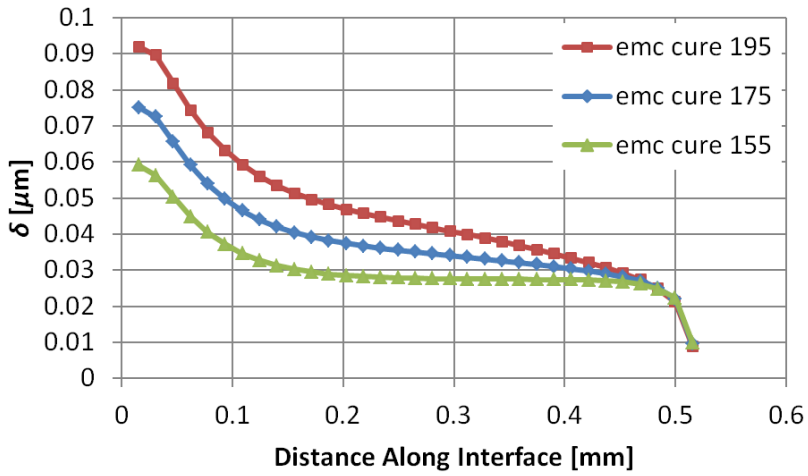

Figure 7.24: Normal separation with varying EMC cure temperature [°].

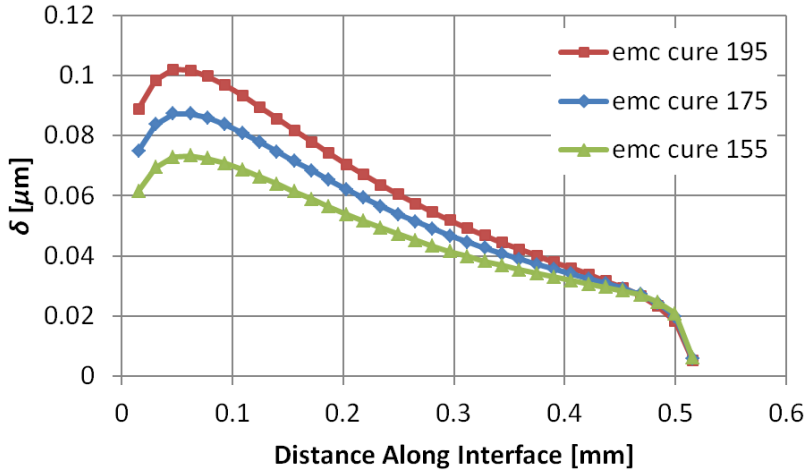

Figure 7.25: Shear separation with varying EMC cure temperature [°].

The EMC cure temperature has a large effect on copper/EMC separation because the interfacial stresses are incurred during this final thermal excursion. Selecting an EMC material with a lower cure temperature is an effective way to directly reduce interfacial stresses.

7.8 SOIC Design Guidelines

Several of the parameters investigated have significant effects on the interfacial separations. Though none of the combinations indicate failure will occur after fabrication, identifying trends can help avoid subsequent failure during thermal cycling. The following design guidelines can be used to increase mechanical reliability in the SOIC package.

1. The die thickness should be kept as small as possible.
2. If the interface length is increased, a crack that propagates may arrest before reaching the end of the copper pad.
3. The overall package may be thinned significantly without any noticeable consequence with respect to reliability.
4. Die attach cure temperature does not significantly affect interfacial separation.
5. An EMC material with lower cure temperature is preferred to reduce stresses at the interface.

CHAPTER 8

CONCLUSIONS

The primary objective of this work was to develop a predictive tool for investigating interfacial delamination using cohesive zone modeling. First, critical SERR for a copper/EMC interface was experimentally determined through interfacial fracture experiments. Experiments were carried out at multiple mode-mixity to characterize G_C with respect to ψ. Using G_C measurements and load-displacement data from these experiments, cohesive zone parameters were determined to simulate the copper/EMC interface by mimicking load-displacement data from the interfacial fracture experiments. A 2D SOIC model was prepared and appropriate material models were identified. A process model was created by modeling thermal excursions and using element birth and death to simulate the SOIC fabrication procedure. A fracture mechanics approach was performed on the SOIC by creating a pre-crack and evaluating the SERR. Cohesive zone elements were placed along the interface, and CZ fracture results were compared to fracture mechanics results. Using the CZ model, a parametric study was performed by modifying various parameters and comparing results. The following conclusions are based on this study.

8.1 Experimental Characterization of the Interface

To characterize the interface, DCB and FPB tests were performed. For both tests, G_C was calculated using VCCT and verified with analytical equations. Both experiments provided good results for G_C. As anticipated, the DCB test produced a mode-mixity

close to 0°, but the mode-mixity for the FPB test was lower than expected. The FPB test was intended to produce mode-mixity close to 45° as commonly seen in thin-film delamination tests. Due to the large difference in thickness between copper and EMC layers, the mode-mixity for the FPB test was only 14.0°. As a result, the Hutchinson and Suo model fit in Fig. 5.15 is not a strong fit. Future work should include an interfacial fracture test at higher mode-mixity.

8.2 Determination of Cohesive Zone Parameters

Cohesive zone parameters were successfully acquired for the copper/EMC interface. Fig. 6.4 – Fig. 6.6 show good fits between simulated and experimental load-displacement data for both DCB and FPB. In the FPB results, the CZ model does not capture crack propagation through the EMC, though a future model could insert CZ elements in the EMC to accomplish this. Small variations between experimental and model data may be caused by frictional and plasticity effects. Thus the general CZ design procedure was validated and it may be used to determine parameters for other interfaces. Also, the CZ parameters determined for this copper/EMC interface may be inserted into other models at interfaces between copper leadframe and epoxy molding compound.

8.3 Copper/EMC Delamination in SOIC Package

After fully characterizing the mixed-mode CZ model for the copper/EMC interface, an SOIC model was prepared to investigate delamination in a microelectronic package. A process model was developed to simulate thermal excursions associated with

fabrication of the package. A fracture mechanics analysis and a cohesive zone analysis of copper/EMC interfacial fracture both agreed that no delamination would result from package fabrication. It is more likely that interfacial delamination will occur as a result of fatigue loading during thermal cycling. The cohesive zone analysis performed here is a first step toward a model that can incorporate fatigue loading.

Though no damage was incurred during process modeling with CZ elements, the interfacial separations can be used effectively to compare the effects of various packaging parameters. The design guidelines resulting from the parametric study are summarized below.

1. Die thickness should be kept as small as possible.
2. An EMC material with lower cure temperature is preferred.

8.4 Research Contributions

This work represents a significant advance in the use of cohesive zone modeling for studying delamination in copper/mold compound interface in microelectronic packaging. The CZ parameter design procedure presented here may be used to develop a mixed-mode cohesive zone law for any interface. Within the field of microelectronic packaging, the procedure can be used for several common packaging interfaces, such as silicon/epoxy molding compound, silicon/underfill, etc.

The mixed-mode CZ model can be used as a predictive model to determine if loading conditions will cause interfacial cracking in the package. The fully-defined CZ

model may be used in other geometries that contain a copper/EMC interface, such as flip-chip packages, stacked IC packages, 3D IC packages, and multi-chip modules. Eventually, multiple interfaces may be modeled in the same package by defining mixed-mode CZ models for each interface.

8.5 Future Work

Future work on studying interfacial delamination through cohesive zone models will continue with the following goals in mind:

1. An additional interfacial fracture test such as ENF or 4ENF should be performed to characterize critical SERR near mode II. Additional data points will provide a better fit to the Hutchinson and Suo model and will validate the selection of the mixed-mode cohesive zone parameters.
2. Residual thermo-mechanical stresses, cure shrinkage, and copper plasticity may be considered in calculations of critical SERR. Copper plasticity may affect measurements since the copper layer in the bimaterial specimens is thin relative to the EMC layer. Residual stresses and cure shrinkage may contribute to stresses near the crack tip and raise the measured critical SERR.
3. Copper/EMC adhesion is affected by many factors, such as moisture, temperature, and surface roughness. The CZ model may be modified to simulate these effects.
4. Since no delamination is predicted to occur after fabrication, a new study should investigate fatigue failure of the copper/EMC interface. Far in the future, a CZ

model may be able to predict interfacial failure under cyclic loading. Appropriate elastic-plastic and viscoplastic material models should be considered.

REFERENCES

[1] R. R. Tummala and M. Swaminathan, *System on Package: Miniaturization of the Entire System*. New York: McGraw-Hill, 2008.

[2] R. R. Tummala, *Fundamentals of Microsystems Packaging*. New York: Mcgraw-hill, 1997.

[3] A. Nishimura, I. Hirose, and N. Tanaka, "A New Method for Measuring Adhesion Strength of IC Molding Compounds," *Journal of Electronic Packaging,* vol. 114, p. 407, 1992.

[4] L. Sheng, M. Yuhai, and T. Y. Wu, "Bimaterial interfacial crack growth as a function of mode-mixity," *Components, Packaging, and Manufacturing Technology, Part A, IEEE Transactions on,* vol. 18, pp. 618-626, 1995.

[5] H. C. Cao and A. G. Evans, "An experimental study of the fracture resistance of bimaterial interfaces," *Mechanics of Materials,* vol. 7, pp. 295-304, 6// 1989.

[6] K. M. Liechti and Y. S. Chai, "Biaxial Loading Experiments for Determining Interfacial Fracture Toughness," *Journal of Applied Mechanics,* vol. 58, pp. 680-687, 1991.

[7] N. P. O'Dowd, C. F. Shih, and M. G. Stout, "Test geometries for measuring interfacial fracture toughness," *International Journal of Solids and Structures,* vol. 29, pp. 571-589, // 1992.

[8] B. D. Davidson and V. Sundararaman, "A single leg bending test for interfacial fracture toughness determination," *International Journal of Fracture,* vol. 78, pp. 193-210, 1996/06/01 1996.

[9] P. P. L. Matos, R. M. McMeeking, P. G. Charalambides, and M. D. Drory, "A method for calculating stress intensities in bimaterial fracture," *International Journal of Fracture,* vol. 40, pp. 235-254, 1989/08/01 1989.

[10] J. R. Rice, "A path independent integral and the approximate analysis of strain concentration by notches and cracks," *Journal of applied mechanics*, vol. 35, pp. 379-386, 1968.

[11] M. Toya, "On mode I and mode II energy release rates of an interface crack," *International Journal of Fracture*, vol. 56, pp. 345-352, 1992/08/01 1992.

[12] W. T. Chow and S. N. Atluri, "Finite element calculation of stress intensity factors for interfacial crack using virtual crack closure integral," *Computational Mechanics*, vol. 16, pp. 417-425, 1995/11/01 1995.

[13] L. Durix, M. Dreßler, D. Coutellier, and B. Wunderle, "On the development of a modified button shear specimen to characterize the mixed mode delamination toughness," *Engineering Fracture Mechanics*, vol. 84, pp. 25-40, 2012.

[14] W. Szeto, M. Xie, J. Kim, M. Yuen, P. Tong, and S. Yi, "Interface failure criterion of button shear test as a means of interface adhesion measurement in plastic packages," in *Electronic Materials and Packaging, 2000.(EMAP 2000). International Symposium on*, 2000, pp. 263-268.

[15] J.-K. Kim, M. Lebbaj, J. H. Liu, J. H. Kim, and M. M. Yuen, "Interface adhesion between copper lead frame and epoxy moulding compound: effects of surface finish, oxidation and dimples," in *Electronic Components & Technology Conference, 2000. 2000 Proceedings. 50th*, 2000, pp. 601-608.

[16] W. K. Lam, T. S. Yeung, A. Teng, and M. M. F. Yuen, "A method for evaluating delamination between epoxy moulding compounds and different plated leadframes," in *Electronic Materials and Packaging, 2000. (EMAP 2000). International Symposium on*, 2000, pp. 214-219.

[17] W. Van Driel, M. Van Gils, R. B. van Silfhout, and G. Zhang, "Prediction of delamination related IC & packaging reliability problems," *Microelectronics Reliability*, vol. 45, pp. 1633-1638, 2005.

[18] X. Guofeng, Q. Fei, Z. Wenhui, G. Cha, and M. Xiaobo, "Interfacial delamination and reliability design of exposed pad packages," in *Electronic Packaging Technology and High Density Packaging (ICEPT-HDP), 2012 13th International Conference on*, 2012, pp. 588-594.

[19] W. Xie and S. K. Sitaraman, "Investigation of interfacial delamination of a copper-epoxy interface under monotonic and cyclic loading: experimental characterization," *Advanced Packaging, IEEE Transactions on,* vol. 26, pp. 447-452, 2003.

[20] X. Liu, Q. Chen, V. Sundaram, R. R. Tummala, and S. K. Sitaraman, "Failure analysis of through-silicon vias in free-standing wafer under thermal-shock test," *Microelectronics Reliability,* vol. 53, pp. 70-78, 1// 2013.

[21] R. J. Harries and S. K. Sitaraman, "Numerical modeling of interfacial delamination propagation in a novel peripheral array package," *Components and Packaging Technologies, IEEE Transactions on,* vol. 24, pp. 256-264, 2001.

[22] V. Sundararaman and S. K. Sitaraman, "Interfacial fracture toughness for delamination growth prediction in a novel peripheral array package," *Components and Packaging Technologies, IEEE Transactions on,* vol. 24, pp. 265-270, 2001.

[23] W. Xie and S. K. Sitaraman, "Investigation of interfacial delamination of a copper-epoxy interface under monotonic and cyclic loading: modeling and evaluation," *Advanced Packaging, IEEE Transactions on,* vol. 26, pp. 441-446, 2003.

[24] H. Mei, S. Gowrishankar, K. M. Liechti, and R. Huang, "Initiation and propagation of interfacial delamination in integrated thin-film structures," in *Thermal and Thermomechanical Phenomena in Electronic Systems (ITherm), 2010 12th IEEE Intersociety Conference on*, 2010, pp. 1-8.

[25] S. Li, M. Thouless, A. Waas, J. Schroeder, and P. Zavattieri, "Mixed-mode cohesive-zone models for fracture of an adhesively bonded polymer–matrix composite," *Engineering fracture mechanics,* vol. 73, pp. 64-78, 2006.

[26] P. Rahul-Kumar, A. Jagota, S. Bennison, S. Saigal, and S. Muralidhar, "Polymer interfacial fracture simulations using cohesive elements," *Acta materialia,* vol. 47, pp. 4161-4169, 1999.

[27] S. Raghavan, I. Schmadlak, G. Leal, and S. K. Sitaraman, "Framework to Extract Cohesive Zone Parameters Using Double Cantilever Beam and Four-Point Bend Fracture Tests," in *Thermal, Mechanical and Multi-Physics Simulation and*

Experiments in Microelectronics and Microsystems (EuroSimE), 2014 15th International Conference on, 2014.

[28] G. R. Irwin, "Fracture dynamics," *Fracturing of metals*, vol. 147, p. 166, 1948.

[29] E. Orowan, "Fracture and Strength of Solids," *Reports on Progress in Physics*, vol. XII, pp. 185-232, 1948.

[30] T. L. Anderson, *Fracture Mechanics: Fundamentals and Applications, Third Edition*: Taylor & Francis, 2005.

[31] H. T. Tran, M. H. Shirangi, X. Pang, and A. A. Volinsky, "Temperature, moisture and mode-mixity effects on copper leadframe/EMC interfacial fracture toughness," *International Journal of Fracture*, vol. 185, pp. 115-127, 2014/01/01 2013.

[32] E. F. Rybicki and M. F. Kanninen, "A finite element calculation of stress intensity factors by a modified crack closure integral," *Engineering Fracture Mechanics*, vol. 9, pp. 931-938, // 1977.

[33] R. Krueger, "Virtual crack closure technique: History, approach, and applications," *Applied Mechanics Reviews*, vol. 57, pp. 109-143, 2004.

[34] M. L. Williams, "The stresses around a fault or crack in dissimilar media," *Bulletin of the Seismological Society of America*, vol. 49, pp. 199-204, April 1, 1959 1959.

[35] A. Agrawal and A. M. Karlsson, "Obtaining mode mixity for a bimaterial interface crack using the virtual crack closure technique," *International Journal of Fracture*, vol. 141, pp. 75-98, 2006/09/01 2006.

[36] J. R. Rice, "Elastic Fracture Mechanics Concepts for Interfacial Cracks," *Journal of Applied Mechanics*, vol. 55, p. 98, 1988.

[37] J. Hutchinson and Z. Suo, "Mixed mode cracking in layered materials," *Advances in applied mechanics*, vol. 29, p. 191, 1992.

[38] J. Yau, S. Wang, and H. Corten, "A mixed-mode crack analysis of isotropic solids using conservation laws of elasticity," *Journal of Applied Mechanics,* vol. 47, pp. 335-341, 1980.

[39] M. Elices, G. Guinea, J. Gomez, and J. Planas, "The cohesive zone model: advantages, limitations and challenges," *Engineering fracture mechanics,* vol. 69, pp. 137-163, 2002.

[40] G. Alfano and M. Crisfield, "Finite element interface models for the delamination analysis of laminated composites: mechanical and computational issues," *International journal for numerical methods in engineering,* vol. 50, pp. 1701-1736, 2001.

[41] A. Xiao, H. Pape, B. Wunderle, K. Jansen, J. de Vreugd, and L. Ernst, "Interfacial fracture properties and failure modeling for microelectronics," in *Electronic Components and Technology Conference, 2008. ECTC 2008. 58th*, 2008, pp. 1724-1730.

[42] L. Xu, X. Lu, J. Liu, X. Du, Y. Zhang, and Z. Cheng, "Adhesion behavior between epoxy molding compound and different leadframes in plastic packaging," in *Electronic Packaging Technology & High Density Packaging, 2009. ICEPT-HDP'09. International Conference on*, 2009, pp. 1039-1042.

[43] M. Shirangi, W. Müller, and B. Michel, "Determination of Copper/EMC interface fracture toughness during manufacturing, moisture preconditioning and solder reflow process of semiconductor packages," in *ICF12, Ottawa 2009*, 2013.

[44] G. T. Ostrowicki and S. K. Sitaraman, "Magnetically actuated peel test for thin films," *Thin Solid Films,* vol. 520, pp. 3987-3993, 3/30/ 2012.

[45] M. B. Modi and S. K. Sitaraman, "Interfacial fracture toughness measurement for thin film interfaces," *Engineering Fracture Mechanics,* vol. 71, pp. 1219-1234, 6// 2004.

[46] W. O. Soboyejo, G. Y. Lu, S. Chengalva, J. Zhang, and V. Kenner, "A modified mixed-mode bending specimen for the interfacial fracture testing of dissimilar materials," *Fatigue & Fracture of Engineering Materials & Structures,* vol. 22, pp. 799-810, 1999.

[47] V. Sundararaman and B. D. Davidson, "An unsymmetric double cantilever beam test for interfacial fracture toughness determination," *International Journal of Solids and Structures,* vol. 34, pp. 799-817, 3// 1997.

[48] F. Xiao, C. Y. Hui, and E. J. Kramer, "Analysis of a mixed mode fracture specimen: the asymmetric double cantilever beam," *Journal of Materials Science,* vol. 28, pp. 5620-5629, 1993/01/01 1993.

[49] P. G. Charalambides, J. Lund, A. G. Evans, and R. M. McMeeking, "A Test Specimen for Determining the Fracture Resistance of Bimaterial Interfaces," *Journal of Applied Mechanics,* vol. 56, p. 77, 1989.

[50] S. Noijen, O. van der Sluis, and P. Timmermans, "An extensive investigation of the four point bending test for interface characterization," in *Thermal, Mechanical and Multi-Physics Simulation and Experiments in Microelectronics and Microsystems (EuroSimE), 2012 13th International Conference on*, 2012, pp. 1/9-9/9.

[51] M. Shirangi, B. Wunderle, O. Wittler, H. Walter, and B. Michel, "Modeling cure shrinkage and viscoelasticity to enhance the numerical methods for predicting delamination in semiconductor packages," in *Thermal, Mechanical and Multi-Physics simulation and Experiments in Microelectronics and Microsystems, 2009. EuroSimE 2009. 10th International Conference on*, 2009, pp. 1-8.